LUND UNIVERSITY

Characterization of Coniferyl Aldehyde Dehydrogenase and cofactor regeneration with NADH oxidase in the biotransformation from FFCA to FDCA

Chengsi Li

8/28/2024

Master's Thesis

Division of Biotechnology

Examiner
Rajni Hatti-Kaul

Supervisor
Mohamed Ismail

Abstract

This thesis focuses on the characterization of Coniferyl aldehyde dehydrogenase (CALDH) and cofactor regeneration involved in the biotransformation process from 5-Formyl-2-furancarboxylic Acid (FFCA) to 2,5-furandicarboxylic acid (FDCA) using NADH oxidases. FDCA is a building block of bio-based polymers like polyethylene furanoate (PEF), which serves as a sustainable alternative to traditional Polyethylene terephthalate (PET) plastics. However, the biocatalytic process faces efficiency challenges due to, for example, the limited availability of cofactors like NAD^+, which are essential for the catalytic activity of enzymes involved in this conversion. In this study, the enzyme CALDH (previously characterized from *Gluconobacter oxydans* DSM50049 genome) was purified and characterized to determine its cofactor and substrate specificity. CALDH was characterized to use HMF, FFCA, and furfural as substrates. The conversion of FFCA to FDCA and the catalytic ability of CALDH were assessed at different enzyme and substrate concentrations. Additionally, a system for NAD+ regeneration with Nox (NADH oxidase) was assayed, which improved FDCA yield threefold. The results demonstrated that the cofactor regeneration system significantly improved the yield of FDCA, offering a potential solution for the production of bio-based plastics.

Keywords

5-hydroxymethylfurfural, 2,5-furandicarboxylic acid, NADH oxidase, Coniferyl aldehyde dehydrogenase, biotransformation, cofactor regeneration, bio-based plastics.

Popular Abstract

The environmental impact of fossil-based plastics has become increasingly alarming, with global plastic production climbing from 370 million tonnes in 2018 to 400 million tonnes in 2022. Despite the urgent need for change, fossil-based plastics still dominate the market, accounting for 90.6% of total production in 2022, while bio-based plastics represent only a tiny fraction at 0.5%. The small amount of bioplastics highlights the vast potential and necessity for expanding the development of sustainable alternatives. One particularly promising biobased material is polyethylene furanoate (PEF), which is produced from 2,5-furandicarboxylic acid (FDCA). Unlike traditional PET, PEF offers better barrier properties and is recyclable, making it an ideal candidate for the next generation of sustainable plastics.

The parent molecule for FDCA is 5-hydroxymethylfurfural (HMF), which is obtained by dehydration of fructose or glucose, the components of sugar. Transformation of HMF to FDCA requires a series of 3 oxidation reactions that can be achieved by chemical or enzymatic catalysis. Chemical catalysis using noble metal catalysts is not environment friendly. On the other hand, enzymatic catalysis occurs under mild conditions but needs help of cofactors for transfer of electrons. The cofactor needs to be regenerated for its repeated use. A commonly used cofactor in living systems is Nicotinamide adenine dinucleotide (Phosphate) oxidized form (NAD(P)+) that is reduced to Nicotinamide adenine dinucleotide (Phosphate) reduced form (NAD(P)H) during electron transfer.

Earlier research at Division of Biotechnology, Lund University has shown that bacteria called *Gluconobacter oxydans* catalyses two of the three oxidation steps from HMF to FDCA. This thesis focuses on characterizing the enzyme Coniferyl Aldehyde Dehydrogenase (CALDH) from *Gluconobacter oxydans* that catalyses the last oxidation step for transforming 5-formyl-2-furancarboxylic acid (FFCA) to FDCA and studying the effect of cofactor regeneration using another enzyme NADH oxidase. The enzyme was purified and its activity with different substrates and cofactors (NAD+/NADP+) studied. Additionally, a new system was developed to recycle NAD+ and improved FDCA yield threefold. The results are promising, showing that this cofactor regeneration system could greatly enhance the efficiency of producing FDCA on a larger scale.

Table of contents

Abstract i
Keywords i
Popular Abstract ii
Table of contents iii
List of acronyms and abbreviations iv
1 Introduction 5
1.1 From biomass to plastic Background 5
1.2 Related work on FDCA production and Problems 6
1.3 Aldehyde dehydrogenase and Coniferyl aldehyde dehydrogenase 7
1.4 NADH oxidase for cofactor regeneration 8
1.5 Goals 10
2 Materials and Methods 10
2.1 Materials 10
2.2 Bacteria cultivation, proteins expression and purification 10
2.2.1 Cultivation and induction of protein expression 10
2.2.2 Protein Purification 11
2.3 Characterization of enzymes and cofactor regeneration with purified enzyme 12
2.3.1 Characterization of CALDH 12
2.3.2 Activity assay for Nox 13
2.3.3 Cofactor regeneration assay 13
2.4 Co-expression vector design for Nox and mbp-CALDH 14
2.4.1 Primer Design 14
2.4.2 Plasmid Extraction and Gene Amplification 14
2.4.3 Digestion, Ligation and Gibson Assembly 17
2.4.4 Transformation and Colony PCR 17
3 Results and Analysis 18
3.1 Selection of NADH oxidase 18
3.2 Protein expression and purification 19
3.3 Characterization of mbp-CALDH 24
3.3.1 Cofactor Specificity 24
3.3.2 Substrate Specificity 24
3.3.3 mbp-CALDH activity at different substrate (FFCA) concentration 28
3.3.4 FFCA conversion at different enzyme concentration 30
3.4 FFCA conversion with cofactor regeneration 31
3.5 Co-Expression Vector Design for NOX and mbp-CALDH 31
4 Conclusions and Future work 32
5 Acknowledge 33
References 34
Appendix A: 41

List of acronyms and abbreviations

CALDH	Coniferyl Aldehyde Dehydrogenase
DFF	2,5-diformylfuran
FAD	flavin adenine dinucleotide
FDCA	2,5-furandicarboxylic acid
FFCA	5-Formyl-2-furancarboxylic Acid
HMF	5-hydroxymethylfurfural
HMFCA	5-hydroxymethyl-2-furancarboxylic acid
NADH	Nicotinamide adenine dinucleotide (reduced form)
NAD^+	Nicotinamide adenine dinucleotide (oxidized form)
NADPH	Nicotinamide adenine dinucleotide phosphate (reduced form)
$NADP^+$	Nicotinamide adenine dinucleotide phosphate (oxidized form)
NOX	NADH oxidase
PCR	Polymerase chain reaction
PEF	polyethylene furanoate
PET	polyethylene terephthalate
SUMO	Small Ubiquitin-like Modifier

1 Introduction

1.1 From biomass to plastic Background

Plastic is an indispensable material widely used across various fields. Global plastic production has skyrocketed in recent decades and reaches approximately 400.3 million tons in 2022 [1]. However, only about 9% of all plastic ever produced has been recycled, with the vast majority—nearly 79%—ending up in landfills, incineration, or the environment as waste. The total plastic production in Europe is 58.7 million tons, 47.8 million tons were based on fossil fuels, which contributes significantly to greenhouse gas emissions [2]. Based on current trends, greenhouse gas emissions from plastic production and disposal are estimated to reach 1.34 Gt annually by 2030 [3]. Using bio-based materials as the feedstock for plastic production facilitates the industrial transition from fossil fuel dependence to more sustainable practices. Biomass is a rich and sustainable source of hexose including glucose and fructose, which can be further converted to building blocks of biopolymers through biotechnology methods [4].

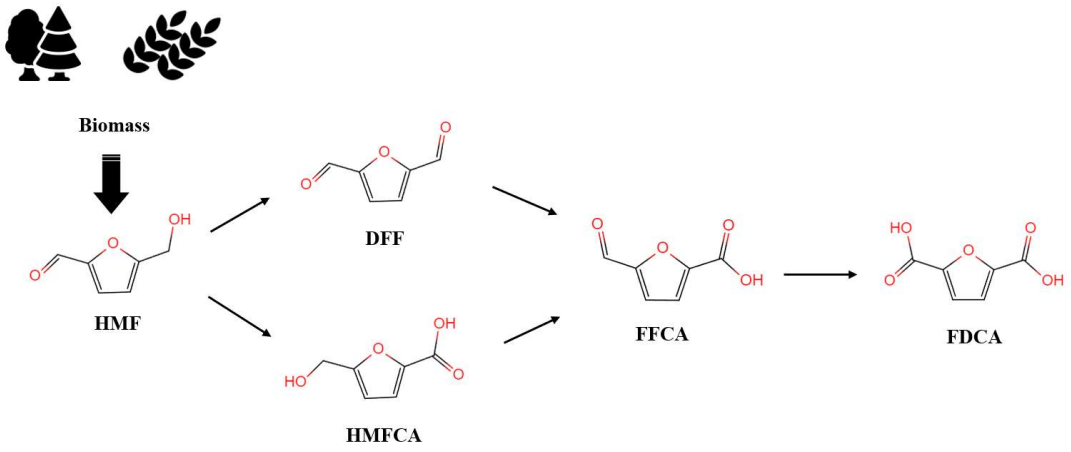

Scheme 1. Different routes for FDCA production. HMF: 5-hydroxymethylfurfural. DFF: 2,5-diformylfuran. HMFCA: 5-hydroxymethyl-2-furancarboxylic acid. FFCA: 5-Formyl-2-furancarboxylic Acid. FDCA: 2,5-furandicarboxylic acid.

5-hydroxymethylfurfural (5-HMF) which is obtained by the dehydration of hexose has a potential as a platform molecule for production of 2,5-furandicarboxylic acid (FDCA), 2,5-diformylfuran (DFF), levulinic acid, furfuryl alcohol and other chemicals [5]. Considering the policies on the limitation of plastic consumption along with carbon footprint and the transition to sustainable economy and industries, the FDCA was ranked by the U. S. Department of Energy (DOE) as the second bio-based compound with high future capacity. Hence, expected FDCA market potential

is high and the market value is estimated to grow from $441.5 million in 2020 to $857.3 million by 2028 [6, 7]. FDCA is an essential bio-based chemical which can be used to produce polyethylene furanoate (PEF). PEF is a bio-based plastic with better thermal and mechanical properties than polyethylene terephthalate (PET) [8]. It has placed PEF in a strategic position to offer more sustainable solutions to industries.

5-HMF consists of a furan ring with an aldehyde group at the 2-position and a hydroxymethyl group at the 5-position. The conversion of HMF to FDCA involves a series of oxidation reactions, with two different strategies based on the oxidation order of functional groups (Scheme 1). In the first strategy, the hydroxymethyl group of 5-HMF is initially oxidized to an aldehyde group which forms DFF. Then each aldehyde group on DFF is oxidized to carboxylic acid groups, first generates 5-Formyl-2-furancarboxylic Acid (FFCA) and eventually results in FDCA. In another approach, the aldehyde group of 5-HMF is oxidized to form 5-hydroxymethyl-2-furancarboxylic acid (HMFCA), followed by the oxidation of the hydroxyl group to yield FFCA which is subsequently oxidized to FDCA [9].

5-HMF can be oxidized to FDCA using noble metal catalysts such as gold (Au), platinum (Pt), palladium (Pd), and ruthenium (Ru) under alkaline conditions [10]. However, this process presents several significant challenges. The addition of a base leads to the formation of byproduct salts, necessitating subsequent separation steps. The reaction also requires high temperatures and the use of costly noble metal catalysts, which collectively elevate the operational costs and complicate the downstream process [11]. Biocatalysis with whole cells or enzymes can address these shortcomings, providing another potential solution.

1.2 Related work on FDCA production and Problems

Koopman *et al.* identified a *hmfH* gene that encodes an oxidoreductase from *Cupriavidus basilensis* HMF14, which can catalyze all three oxidation steps from HMF to FDCA [12]. Then to achieve whole cell catalysis, the *hmfH* gene was introduced into *Pseudomonas putida* S12, a strain that is known for its tolerance to toxic substrates[13]. FDCA production through biotransformation has been achieved, however, the process is inefficient. Fed-batch fermentation experiments showed a 97% FDCA yield from HMF after 117.4 hours of cultivation [14]. To further enhance efficiency of whole cell catalysis, Yuan *et al*. overexpressed *hmfH* in *Raoultella ornithinolytica* BF60 and reached 93.6% FDCA yield from HMF in 120 hours. Results showed the accumulation of HMFCA and FFCA during the fermentation, suggesting that the two

reactions involved in the oxidation of HMFCA and FFCA are rate-limiting steps in FDCA production [15, 16].

Due to the toxicity of HMF to enzymes, reports on enzymatic catalysis for the production of FDCA are relatively limited. Since the conversion of HMF to FDCA requires a series of oxidation reactions, it is typically catalyzed with enzyme cascades [11]. For example, Krysof reported a method that use a combination of lipases and a silica-based immobilized TEMPO (2,2,6,6-tetramethylpiperidine-1-oxyl) catalyst. TEMPO first oxidized the aldehyde groups in HMF to yield 2,5-diformylfuran (DFF). Then, lipases are used to generate organic peracids *in situ*, which then selectively oxidized DFF to FDCA [17]. McKenna used galactose oxidase and aldehyde oxidase PaoABC achieved one-pot conversion from HMF to FDCA and had a 97% conversion rate of 10mM HMF in 1 hour [18]. In addition, Karich *et al.* achieved a biotransformation of HMF to FDCA by utilizing aryl alcohol oxidase, peroxygenase, and galactose oxidase from different sources [19].

Sayed *et al.* utilized *Gluconobacter oxydans* DSM 50049 as whole cell catalyst for the conversion of HMF to HMFCA. Under optimized conditions at pH 7 and 30 °C, a 100% conversion of HMF was achieved in 12 hours of reaction time [20]. The subsequent work identified a novel Coniferyl Aldehyde Dehydrogenase (CALDH) from *Gluconobacter oxydans* DSM 50049, which is responsible for the oxidation of HMF. Additionally, CALDH has been found to have the capability to oxidize FFCA to FDCA, a process significantly enhanced by the addition of the cofactor Nicotinamide adenine dinucleotide (NAD^+), which can be a potential solution of the speed-limiting step of FDCA production. However, due to the inability to purify CALDH in the pervious study, crude lysate was used for research, which introduces certain limitations to the experimental results.

1.3 Aldehyde dehydrogenase and Coniferyl aldehyde dehydrogenase

Aldehyde dehydrogenases (ALDHs) (EC 1.2.1.3, EC 1.2.1.4) are a family of enzymes that catalyze the oxidation of aldehydes to their corresponding carboxylic acids. ALDHs act on a wide range of substrates, including aliphatic and aromatic aldehyde. ALDHs have diverse physiological roles and have been extensively studied in human models. ALDHs oxidize aldehydes to less toxic carboxylic acids, thereby playing a critical role in detoxification [21]. Additionally, ALDHs are involved in biosynthesis, such as converting retinaldehyde to retinoic acid, a hormone crucial for regulating embryonic development, inducing cell differentiation, and exerting anti-tumor effects [22]. Moreover, ALDHs may also protect cells from oxidative damage [23]. Mutations or knockouts of ALDHs in humans are often associated with various diseases [24].

The catalytic activity of ALDHs relies on NAD^+ or $NADP^+$ as cofactors which is converted NADH or NADPH in the process. NAD^+ or $NADP^+$ serves as the electron acceptor during the oxidation of aldehydes (-CHO) to carboxylic acids (-COOH), receiving a proton (H^+) and two electrons ($2e^-$) from the aldehyde. Due to the increased availability of these cofactors as electron acceptors, higher cofactor concentrations can accelerate ALDH oxidation catalyzed by ALDHs. Conversely, elevated levels of NADH or NADPH may inhibit ALDH activity through feedback inhibition mechanisms [24] .

Additionally, there are reports showing that ALDHs can catalyze other reactions. Hong observed that an ALDH from *Bacillus cereus* could oxidize retinal to retinoic acid in the presence of high $NADP^+$ concentrations. However, as the ratio of NADPH to $NADP^+$ increased, the ALDH also exhibited the ability to reduce retinal to retinol [18]. Byers discovered an ALDH from *Vibrio harveyi* that, in addition to oxidizing aliphatic aldehydes, could also reduce acyl-CoA and catalyze the cleavage of thioester bonds [19].

Coniferyl aldehyde dehydrogenase (1.2.1.68) is a specific enzyme belonging to the aldehyde dehydrogenases (ALDH) family. There are not many reports on CALDH, with the first instance of its purification and characterization being from *Pseudomonas* sp. HR199. The natural substrate of coniferyl aldehyde dehydrogenase is coniferyl aldehyde, which is oxidized to ferulic acid in the presence of NAD^+ or $NADP^+$ as cofactor [25]. Like other ALDHs, CALDH can also catalyze aromatic aldehydes, there are reports that CALDH can oxidize benzaldehyde, cinnamaldehyde, vanillin and sinapyl aldehyde. However, it is important to note that aliphatic aldehydes cannot serve as substrates for CALDH [25, 26].

1.4 NADH oxidase for cofactor regeneration

Notably, NAD^+ is a costly chemical, with prices reaching approximately €80 per gram [27], which could substantially increase production costs, especially in large-scale processes. To address this challenge, one potential solution is the introduction of a cofactor regeneration system (Scheme 2). Such a system would continuously recycle NAD^+, thereby reducing the need for constant resupply and creating a more efficient and cost-effective biocatalytic system.

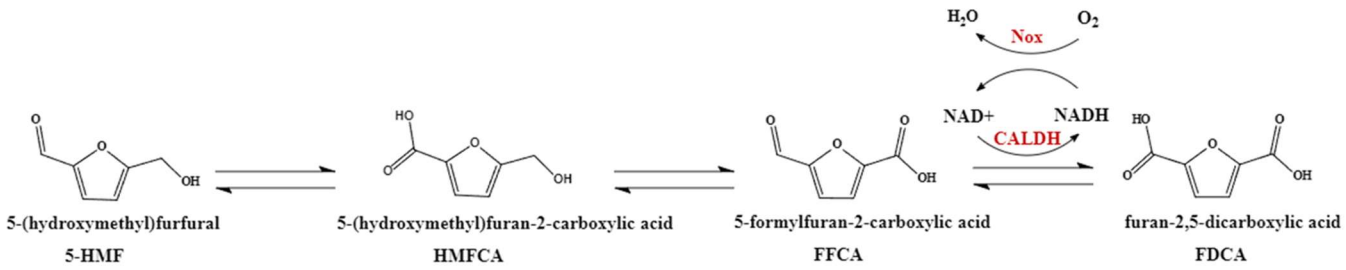

Scheme 2. The cofactor regeneration system in the production of FDCA

Write the cofactor regeneration in the scheme with NAD(P)+ and NAD(P)H

NADH oxidases (Nox) are found across a wide range of organisms, including bacteria, archaea, and eukaryotes. (E.C. 1.6.3.3 and E.C. 1.6.3.4), which can catalyze the oxidation of NADH to NAD^+, with the reduction of O_2 to either H_2O_2 or H_2O. The generation of NAD^+ by NOX is crucial as NAD^+ serves as a vital cofactor in numerous metabolic pathways, including ATP production through oxidative phosphorylation, as well as glycolysis [28]. By oxidizing NADH to NAD^+, NADH oxidase helps protect some aerotolerant anaerobes from the potentially harmful effects of an oxygen-rich environment. This protective mechanism allows these organisms to tolerate and survive in environments where oxygen presents [29].

The activity of Nox is dependent on flavin adenine dinucleotide (FAD) as cofactor. Cysteine 44 is highly conservative in the NADH binding site, which is essential to the formation of water during the oxidation of NADH [30]. The thiol group (-SH) in cysteine can be oxidized to sulfenic acid (-SOH) state and then be reduced back to the thiol form, facilitating the formation of water through the redox cycling (Scheme 3). In this process, the reaction between NADH and oxygen produces hydrogen peroxide, which is reduced by Cys, forming Cys-SOH and water. Then the intermediate Cys-SOH is then further reduced by NADH back to Cys-SH and produces water. As a result, the oxidation of two equivalents of NADH leads to the formation of two equivalents of water [31].

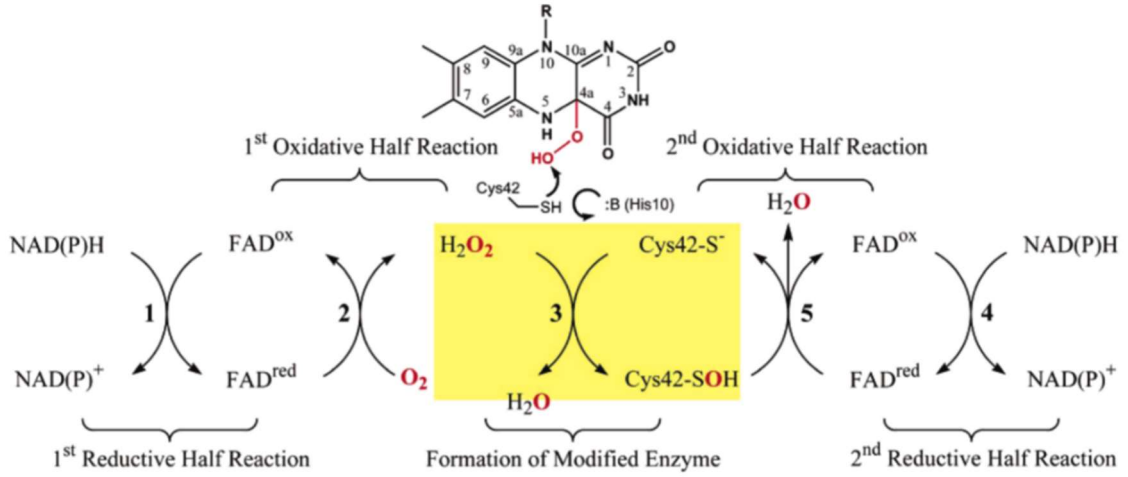

Scheme 3. Illustration of the conservative cysteine function in NADH oxidase [31].

Many researchers have utilized Nox to enhance cofactor regeneration in the biotransformation process that required NAD^+ as cofactor. For example, in the oxidation of l-methionine, a process catalyzed by l-phenylalanine dehydrogenase from *Rhodococcus sp*., the introduction of NADH oxidase from *Lactococcus lactis* for NAD^+ regeneration resulted in a significant increase in the

conversion rate of L-methionine from 28% to 100% [32]. Similarly, in another research, Nox from *Streptococcus mutans* was introduced into *E. coli* combined with xylitol-4-dehydrogenase for the conversion of xylitol to L-xylulose. The presence of Nox not only increased the concentration and productivity of L-xylulose but also led to a rise in intracellular NAD^+ concentration [33]. Moreover, the expression of Nox from *Streptococcus pyogenes* in *E. coli* resulted in a twofold increase in the yield of L-xylulose from L-arabinitol [34]. These examples collectively illustrate the versatility and effectiveness of Nox in improving cofactor regeneration and enhancing productivity in various biotransformation systems.

1.5 Goals

The overall goal of the Master´s project is to evaluate the potential of NAD(P)H oxidase in recycling of the cofactor and in turn improve the efficiency of the CALDH catalyzed oxidation of FFCA to FDCA.

The specific goals of the project are:

- Purification of CALDH and NOx
- Characterization of CALDH with respect to cofactor specificity and substrate specificity, and the effect of varying substrate and enzyme concentrations
- Coupling the CALDH catalyzed FFCA to FDCA reaction with cofactor regeneration by Nox
- Construct co-expression vector for NOX and mbp-CALDH.

2 Materials and Methods

2.1 Materials

The *E. coli* BL21 (DE3) used in experiments was from Sigma-Aldrich (Burlington, USA). The plasmid pET28-a (+), pMAL-c5E and pRSFDuet-1 was from Novagen (Madison, WI, USA). The Luria-Bertani (LB) broth was prepared with 10 g peptone, 5 g sodium chloride and 5 g yeast extract suspended in 1-liter Mili-Q water. The equipment and analysis were specified when mentioned.

2.2 Bacteria cultivation, proteins expression and purification

2.2.1 Cultivation and induction of protein expression

The enzymes in this study were all expressed in the *E. coli* BL21. Four genes encoding for coniferyl aldehyde dehydrogenase were expressed (Table 1): one with the native codon sequence from *G. oxydans* DSM50049 and another with a codon-optimized sequence for *E. coli*. To

increase the solubility of CALDH, the recombinant protein was fused with either Small Ubiquitin-like Modifier (SUMO) or large maltose binding protein (MBP).

To cultivate bacteria and produce the target enzymes listed in Table 1, the preculture of *E. coli* BL21 was cultivated overnight in LB broth with the appropriate antibiotic (50 μg/mL kanamycin or 100 μg/mL Ampicillin（Table 1) at 37°C and 220 RPM. The preculture was then used as an inoculum in a larger volume of LB media with appropriate antibiotic to a starting optical density (OD_{600nm}) of 0.1 and cultivated under the same conditions until the OD_{600nm} reached 0.6. The incubator temperature is lowered to 16°C before starting the induction with isopropyl β-d-1-thiogalactopyranoside addition according to the Table 1. Induction was carried out at 16°C and 180 RPM for 24 hours in orbital Shaker (Kuhner, Switzerland). Cells were harvested by centrifugation at 6,000 RPM (4,307 RCF) for 30 minutes at 4°C with Sorvall Lynx 4000 superspeed centrifuge (Thermo Scientific™, USA) for subsequent protein purification and other purposes.

Table 1. Proteins that expressed in this study, its host cell and expression condition

Enzymes	Expression Host	Antibiotics	Medium	Expression
NADH oxidase	*E. coli* BL21 (DE3)	Kanamycin	Luria-Bertani (LB) broth	0.10 mM IPTG, 16 °C, 24 hours
Coniferyl aldehyde dehydrogenase (Non-optimized)	*E. coli* BL21 (DE3)	Kanamycin	Luria-Bertani (LB) broth	0.15 mM IPTG, 16 °C, 24 hours
Coniferyl aldehyde dehydrogenase (Optimized)	*E. coli* BL21 (DE3)	Kanamycin	Luria-Bertani (LB) broth	0.15 mM IPTG, 16 °C, 24 hours
SUMO-Coniferyl aldehyde dehydrogenase	*E. coli* BL21 (DE3)	Kanamycin	Luria-Bertani (LB) broth	0.15 mM IPTG, 16 °C, 24 hours
MBP-Coniferyl aldehyde dehydrogenase	*E. coli* BL21 (DE3)	Ampicilin	Luria-Bertani (LB) broth	0.15 mM IPTG, 16 °C, 24 hours

2.2.2 Protein Purification

Äkta start protein purification system (Cytiva, USA) was used for enzyme purification. The purification of all proteins in this study is based on the affinity method. The MBPTrap™ HP 1mL (Cytiva, USA) column was used to purify MBP-CALDH. The binding buffer contained 20 mM Tris-HCl, 200 mM NaCl, pH 7.4. The elution buffer was the binding buffer supplemented with 10mM Maltose. First, cells were resuspended in 15mL binding buffer and sonicated with pulse 1 second on and 1 second off, 20% amplitude for 20 minutes with sonicator Fisherbrand™ Model

120 Sonic Dismembrator (Thermo Scientific™, USA). Total lysate was centrifuged at 13,000 RPM (20,217 RCF) for 30 minutes at 4°C with Sorvall Lynx 4000 superspeed centrifuge (Thermo Scientific™, USA). The soluble fraction was collected and filtered with 0.45µm filter. The flow rate for purification was 1mL/min, and after all the soluble fraction flowed through the column, the column was washed with 6 column volume of binding buffer and the isocratic elution with 6 column volume of elution buffer. Five fractions were collected, the volume of each fraction was 1.5 mL.

For the purification of the other enzymes (spNox, CALDH optimized, CALDH non-optimized and SUMO-CALDH), HisTrap™ HP 1mL was used based on the immobilized metal ion affinity chromatography (IMAC). The binding buffer consisted of 20 mM sodium phosphate, 0.5 M NaCl, 20mM imidazole at pH 7.4. The elution buffer was composed of 20 mM sodium phosphate, 0.5 M NaCl and 500 mM imidazole at pH 7.4. The sonication procedure and the settings on Äkta start remained the same as previously described.

After the purification, SDS-PAGE analysis of the purified fractions, soluble fractions, and insoluble fractions was performed using 10% Mini-PROTEAN TGX Stain-Free Precast Gels (BioRad, USA) and a Mini-PROTEAN Tetra Vertical Electrophoresis Cell (BioRad, USA). Electrophoresis was conducted at 80V for 15 minutes, followed by 160V for 45 minutes. The dye solution was prepared by mixing 2-mercaptoethanol and bromophenol blue in a 3:1 ratio with the sample. NanoDrop 1000 Spectrophotometer (Thermo Scientific™, USA) was used to determine the protein concentration based on the absorbance at 280 nm with the molecular weight and extinction coefficient of the corresponding protein.

2.3 Characterization of enzymes and cofactor regeneration with purified enzyme

2.3.1 Characterization of CALDH

The reaction was carried out in a 24-well deep well plate with a reaction volume of 1.5 mL at 30°C and 700 RPM. The deep well plate was incubated in Eppendorf Plate Shaker (Eppendorf, USA). Initially, 5 mM FFCA was used with same concentration of NAD^+ or $NADP^+$ to testify the cofactor specificity. The pH was adjusted to 7.0 using 2M potassium hydroxide, followed by the addition of 150 µM mbp-CALDH, and the volume was adjusted to 1.5 mL with 50mM potassium phosphate buffer (pH 7.0). Next, reactions with different concentrations of FFCA (1 mM, 5 mM, 10 mM, 14 mM, 20 mM, and 50 mM) fixed enzyme concentration of 150 µM; reaction with a fixed substrate concentration (5 mM FFCA) and varying enzyme concentrations (50 µM, 100 µM, 300 µM, 600 µM, and 1.5 mM) were conducted, with the same concentration of NAD^+ and the

volume adjusted similarly. Different substrates (5 mM HMF, HMFCA, FFCA, FDCA, furfural, hydroxybenzaldehyde, benzaldehyde) were also tested under the same conditions.

Samples (20 µL) were taken periodically, mixed with 40 µL of 10% sulfuric acid, diluted to 2 mL with Milli-Q water, filtered through a 0.2 µm filter, and transferred to autosampler vials for HPLC analysis. HPLC was performed using a Bio-Rad fast acid analysis column (100 × 7.8 mm) with a mobile phase of 0.5 mM sulfuric acid at 65°C, with 20 minutes acquisition time and detection at 245 nm UV.

2.3.2 Activity assay for Nox

The activity assay was conducted in a 96-well plate with a total volume of 100 µL per well. The reaction mixture contained 20 µM NADH, 0.050 µM SpNox, and 50 mM potassium phosphate buffer (pH 7.0). The positive control included 1 µM FAD, while the negative controls were: 1) 20 µM NADH, elution buffer and 50 mM potassium phosphate buffer (pH 7.0), 2) a mixture of 20 µM NADH and 50 mM potassium phosphate buffer (pH 7.0), and 3) a mixture of 20 µM NADH, 1 µM FAD, and 50 mM potassium phosphate buffer (pH 7.0). The change in NADH concentration was measured as increase in absorbance at 340 nm using a UV spectrophotometer with a plate reader (BioTek Synergy, Agilent).

2.3.3 Cofactor regeneration assay

In this experiment, FFCA was used as a substrate and FDCA as the expected product catalyzed by mbp-CALDH, limited amount of NAD^+ was added with or without Nox to compare the difference in CALDH reaction rate. The cofactor regeneration in a 24-deep well plate was carried out with a total reaction volume of 1.5 mL per well. The concentration of FFCA was 2mg/mL (14mM), CALDH-mbp 300 µM, Nox 0.15 µM, 0.05 µM NAD^+ in 50mM Potassium Phosphate buffer pH7.0. Additionally, mbp-CALDH preserved in different buffers was used for the activity testing. The enzyme was initially stored in maltose elution buffer containing 20 mM Tris-HCl, 200 mM NaCl, and 10 mM maltose (pH 7.4). Dialysis was used to exchange the buffer to either 50 mM potassium phosphate buffer or 20 mM Tris-HCl buffer. The reaction conditions for each buffer-exchanged enzyme were 300 µM mbp-CALDH, 2 mg/mL (14 mM) FFCA, 0.15 µM Nox, and 0.05 µM NAD^+ in 32 deep well plate and the reaction volume were 1.5mL. The deep well plate was incubated with Eppendorf plate shaker in 30℃, 700RPM.

2.4 Co-expression vector design for Nox and mbp-CALDH

2.4.1 Primer Design

The Nox gene is on plasmids pET-28a (+) (Novagen, Madison, WI, USA) and the mbp-CALDH gene is on pMAL-c5E (Novagen, Madison, WI, USA). To clone them into pRSFDuet-1 plasmid vector (Novagen, Madison, WI, USA), the nox gene and mbp-CALDH gene were amplified through PCR. Then, Gibson assembly and ligation were applied (Scheme 4) to build the co-expression construct.

Primer	Sequence (5'→3')	Tm (℃)	Annealing temp. (℃)
NOX_Duet -F	GGAGATATACCATGGGCAGCAGCCAT	71.0	71
NOX_Duet -R	CCGCAAGCTTTCAATCTTTTGCTCCCAGAG	78.1	
mbp_CALDH -F	ATATACATATGGCAGATCTCATGAAAATCGAAGAAGGTAAAC	70.0	70
mbp_CALDH -R	CAGCGGTTTCTTTACCAGACTCAATCAGAAGATCCGGC	75.4	

The Nox gene has appropriate restriction sites (NcoI and HindIII) on forward and reverse sides, thus when designing primers these restriction sites should be included. The mbp-CALDH gene lacks compatible restriction sites for pRSFDuet-1, Gibson Assembly was applied for plasmid cloning in subsequent steps. Therefore, primers with overlapping sequences between mbp-CALDH and pRSFDuet-1 was designed (Table 2). SnapGene (Dotmatics, USA) was used for stimulating the primer design and plasmid cloning in silico.

Table 2. Primer sequence for gene amplification and sequencing

2.4.2 Plasmid Extraction and Gene Amplification

The *E. coli* DH5α with Nox and the *E. coli* DH5α with mbp-CALDH were cultured overnight in 10mL LB media, and then were used for plasmid extraction with GeneJET Plasmid Miniprep Kit (Thermo Scientific™, USA). The concentration of extracted plasmids was measured with the NanoDrop 1000 Spectrophotometer (Thermo Scientific™, USA).

The Nox and mbp-CALDH genes were individually amplified by Polymerase Chain Reaction (PCR) from plasmids pET-28b (+) and pMAL-c5E with designed primers. The Phusion™ High-Fidelity DNA Polymerase (Thermo Scientific™, USA) was used for the PCR reaction and the annealing temperature was calculated according to the enzyme's specifications. The

concentrations of all components are listed in the Table A1 and the PCR conditions followed the three-step protocol from Thermo Scientific's Phusion™ High-Fidelity DNA Polymerase (Table A2).

The result of PCR was analyzed by gel-electrophoresis using 1% agarose gel stained with GelRed, at 90V for 35 minutes on the instrument PowerPac Basic (Bio-Rad, USA). Then the result was visualized with the GelDoc Go Imaging System (Bio-Rad, USA). The gel with correct size were collected and the DNA fragments were purified from the gel with GeneJET Gel Extraction Kit (Thermo Scientific™, USA).

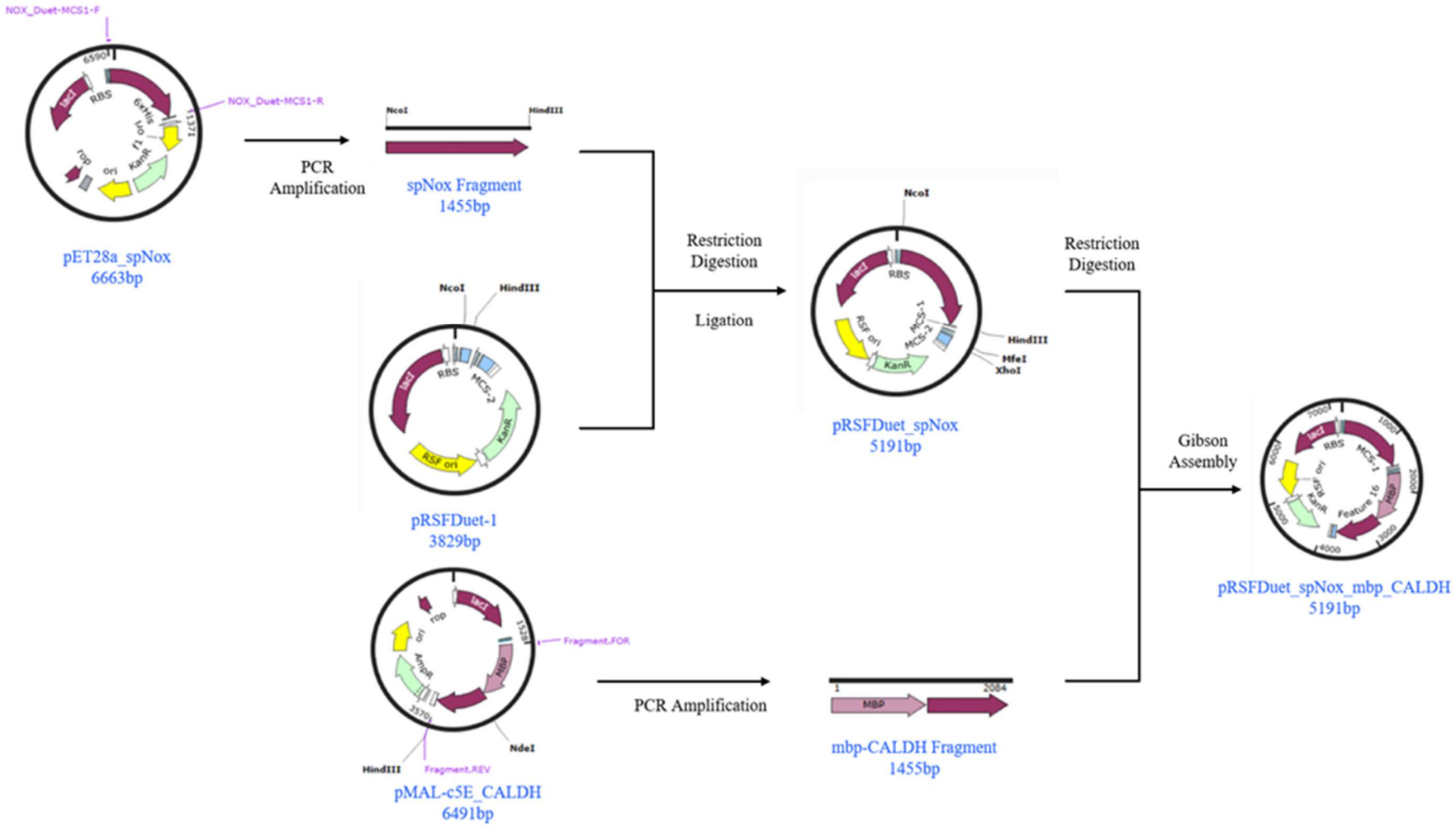

Scheme 4. Co-expression vector design for Nox and mbp-CALDH

2.4.3 Digestion, Ligation and Gibson Assembly

The plasmid pRSFDuet-1 and amplified Nox gene were digested with NcoI and HindIII enzyme (Thermo Scientific™, USA). The plasmid pRSFDuet-Nox and amplified mbp-CALDH gene were digested with MfeI and XhoI enzyme (Thermo Scientific™, USA). The reaction was incubated at 37℃ for 1 hour with Thermocycler (BioRad, USA) and then terminated by inactivation of enzyme at 80℃ for 20 minutes.

Table 3. The component of double enzyme restriction digestion

pSRF-Duet Vector, Nox fragment	pRSFDuet-Nox	Amount
R buffer (Thermo Scientific™, USA)	G buffer (Thermo Scientific™, USA)	2μL
HindIII (Thermo Scientific™, USA)	MfeI (Thermo Scientific™, USA)	1μL
NcoI (Thermo Scientific™, USA)	XhoI (Thermo Scientific™, USA)	2μL
DNA fragments		1μg
Alkalin Phosphatase (Thermo Scientific™, USA)		1μL for plasmid
Water		to 20μL

The cloning of Nox gene into pRSFDuet-1 vector was performed with T4 DNA ligase (New England Biolabs, USA). The quantity of DNA fragments and plasmids were in ratio of 3:1. The reaction was incubated in 16℃ for 16 hours with Thermocycler and then the enzyme was inactivated in 65℃ for 10 minutes.

The Gibson assembly was used to combine mbp-CALDH gene with pRSFDuet-Nox. NEB Gibson assembly master mix (New England Biolabs, USA) which contain 5'exonuclease, DNA polymerase and DNA ligase, was used in this process. DNA fragments and plasmids were in ratio of 3:1 and incubated in a thermocycler at 50°C for 15 minutes.

2.4.4 Transformation and Colony PCR

The construct of pRSFDuet-Nox was verified by colony PCR and Sanger sequencing before proceeding with Gibson assembly. Initially, the ligation product was transformed into *E. coli* DH5α competent cell (Provided by the lab) using the heat shock method. Fifty microliters of competent cells were thawed on ice and mixed with 5 μL of the ligation product, followed by incubation on ice for 30 minutes. The mixture was then heat-shocked at 42°C for 30 seconds and returned to ice for 2 minutes. Subsequently, 950 μL of LB media was added to the transformation mixture and incubated at 220 rpm and 37°C for 1 hour. The cell culture was then spread onto an

LB agar plate containing kanamycin (50 μg/mL) using L-shaped spreaders and air-dried before incubation at 37°C overnight.

Eight random single colonies were picked and resuspended in 12μL of sterile Milli-Q water for colony PCR to confirm the construct. The T7 forward and reverse primers, along with DreamTaq DNA polymerase (Thermo Scientific™, USA) were used for PCR (Table A3). The PCR condition is following the protocol from Thermo Scientific™ (Table A4). The colony with verified construct was cultivated, followed by plasmid extraction. The plasmid containing Nox and mbp-CALDH (pRSFDuet_Nox-mbp-CALDH) was also subjected to the same transformation and confirmation steps as described above. Further verification was performed through Sanger sequencing (Eurofins Genomics Europe Sequencing GmbH) using the T7 forward primer for pRSFDuet-Nox, and the T7 forward primer, T7 reverse primer, and mbp_CALDH-Forward primer for pRSFDuet_Nox-mbp-CALDH. The concentration of plasmid was measured with NanoDrop 1000 Spectrophotometer (Thermo Scientific™, USA).

3 Results and Analysis

3.1 Selection of NADH oxidase

Various NADH oxidases from different bacteria and archaea have been characterized. NADH oxidases from hyperthermophilic microorganisms exhibit high thermal stability, whereas catalytic efficiency is lower than that from non-thermophilic bacteria [35, 36]. Among the different examples of Nox for cofactor regeneration, the water-forming Nox are preferred because the generation of H_2O_2 can inactivate both Nox and the enzymes used in biocatalysis. [37] As mentioned earlier, the conversion of FFCA to FDCA occurs under mild conditions (30°C, pH 7), Therefore, the Nox from *Streptococcus pyogenes* which has characterized kinetic parameters, revealed crystal structure, and applied for cofactor regeneration, has be employed in this study. *Streptococcus pyogenes* is a pathogenic aerotolerant bacteria with a high oxygen tolerance [38]. Nox reduces O_2 to H_2O and regenerates NAD^+, protecting it from oxidative stress in aerobic environments [29]. Nox from *S. pyogenes* is a homodimer with two binding sites for FAD and one binding site for NADH. The size of each subunit is around 50 kDA. Purified SpNox exhibits yellow color, which is attributed to the covalently bound FAD (0.9 ± 0.1 mol per mol subunit) [34].

Table 4. NADH oxidases that was reported in literature

Bacteria	Specific activity (U/mg)	Vmax (U/mg)	Km (μM)	Optimal Temperature (°C)	Optimal pH	Reference
Water forming						
Streptococcus mutans ATCC 25175	281	154	58	35	7	[39]
Streptococcus pyogenes	NA	344	27	55	7	[34]
Lactobacillus reuteri	20.2	168	36	60	5	[30]
Lactobacillus brevis	116	NA	24	40	5.5-7	[40]
Lactobacillus sanfranciscensis	133	39	7	30	5.2	[41]
Hydroxyl Peroxide forming						
Thermus thermophilus HB8	5	NA	4	80	7.2	[35]
Thermotoga hypogea	30	37	7.5	85	7	[36]
Streptococcus mutans	37	NA	50	30	6	[37]

Additionally, by introducing a site-directed mutagenesis from lysine184 to arginine, researchers observed a significant 50% increase in the activity of SpNox. The thermal stability and half-life of the mutant were also improved. The increased activity of the K184R mutant was linked to closer distance between the Cys44 and His11 which reduced from 5.5 Å in the wild type to 4.7 Å. Similarly, the distance between Cys44 and FAD decreased from 4.7 Å in the wild type to 3.8 Å in the K184R mutant, indicating stronger interactions at the active site [42]. This closer proximity to histidine leads to a more stable transition state of cysteine when react with C-4a-hydroperoxide (FADHOOH), therefore enhancing its catalytic efficiency (more details section 1.4). Kinetic analyses showed that the K_m values were similar for both K184R and wild-type SpNox but the catalytic activity of K184R is 50% higher, suggesting that the improved catalytic activity was due to a higher turnover rate rather than higher substrate binding efficiency. [31, 42]

3.2 Protein expression and purification

All the target proteins were successfully expressed in *E. coli* BL21, as confirmed by SDS-PAGE analysis (Figure 3). The Nox was found to be equally distributed between the soluble and insoluble fractions in a 1:1 ratio. Purification of soluble fraction was achieved through IMAC, and two fractions were obtained with high purity: fraction 2 with a concentration of 0.72 mg/mL, and fraction 3 with a concentration of 0.28 mg/mL. Notably, Fraction 2 exhibited yellow color

(Figure 2), which aligns with documented characteristics in the literature. In contrast, Fraction 3 was nearly colorless.

The yellow color observed in the higher concentration fraction is attributed to the presence of FAD. Each spNox monomer contains two domains specifically for FAD binding, and the isoalloxazine ring structure of FAD is responsible for the yellow coloration. This suggests that the enzyme in Fraction 2 is covalently bound to FAD, as indicated by the distinct yellow appearance [34, 43]. To determine whether additional FAD is required to achieve optimal catalytic activity, an enzyme activity assay was conducted using NADH as the substrate in the presence and absence of exogenously added FAD. The results show similar activity of Nox with and without the addition of FAD (Figure A1).

Figure 1. Purified spNox: Fraction 2 (Left), Fraction 3 (Middle); Elution Buffer (Right).

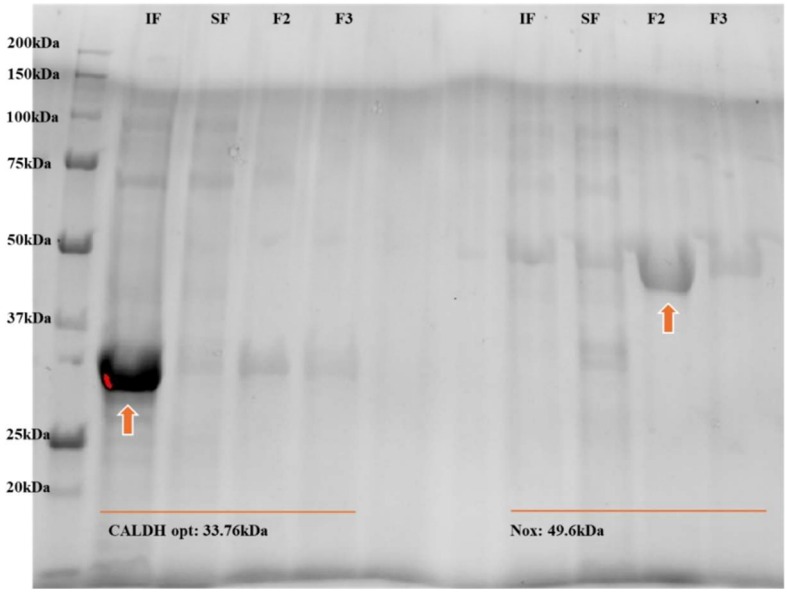

Figure 2. SDS-PAGE result of CALDH opt and spNox. IF: insoluble fraction. SF: soluble fraction. F: fraction.

The codon-optimized CALDH was predominantly distributed in the insoluble fraction of the cell lysate (Figure 3). After purification and concentration by IMAC, the yield of CALDH was notably low. Given this outcome, two additional variants of CALDH were expressed and purified: one maintaining the original sequence amplified from *G. oxydans* and the other fused with a SUMO tag (Figure 4). SDS-PAGE analysis revealed that the non-optimized CALDH was poorly expressed in BL21 (DE3), with the purified fractions containing low amounts of the target protein and impurities. In contrast, the SUMO-CALDH variant was expressed in sufficient quantities in both the soluble and insoluble fractions. Purification by IMAC resulted in a high yield and purity of the enzyme.

The codon optimization of CALDH was intended to enhance expression in the host cells, yet it resulted in the majority of the protein being sequestered in the insoluble fraction. This outcome can be attributed to that optimized codons accelerate translation which interferes with the cellular folding machinery and leads to protein aggregation and insolubility [44]. In comparison, SDS-PAGE analysis showed that non-optimized CALDH was poorly expressed in BL21 (DE3) cells, which shows the necessity of codon optimization for the host bacteria. SUMO is a small protein tag used to enhance the solubility and stability of fusion proteins [45]. By attaching to the target protein, the SUMO tag increases the solubility of the protein in the cell, reducing the formation of aggregates. SUMO-CALDH variant gene was successfully expressed, and the enzyme was purified. However, despite this success in expression and purification, the SUMO-CALDH variant protein failed to catalyze the conversion of FFCA in an activity assay. Fused SUMO tag may interfere with the enzyme's active site or overall conformation [46]. indicating the need to cleave the tag or expression of alternative CALDH variants. Meanwhile, the imidazole in the elution buffer may also lead to the inactivation of enzyme [47]. There is a need to expression of alternative CALDH variants.

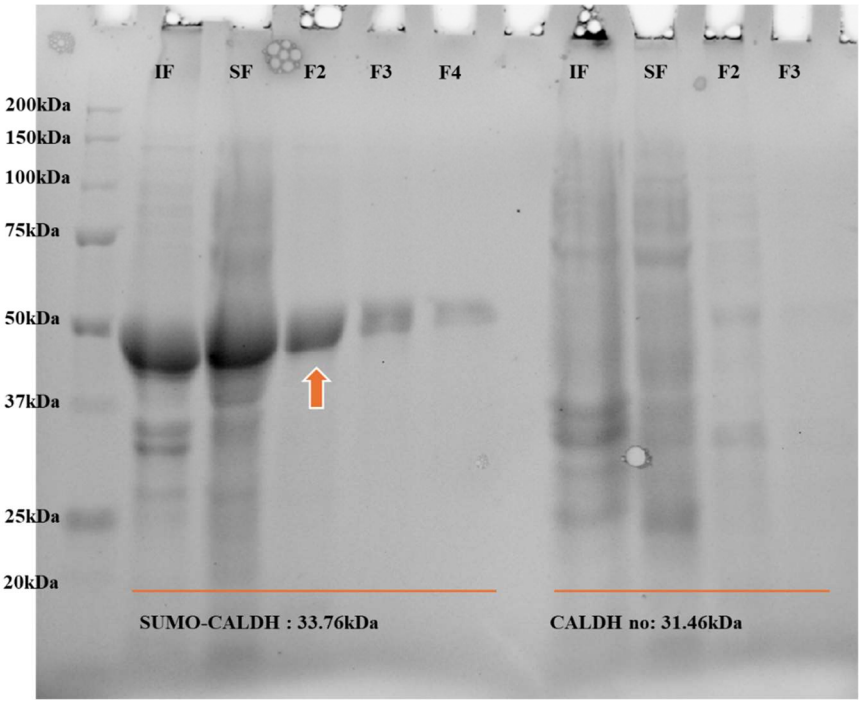

Figure 3. SDS-PAGE result of SUMO-CALDH and non-optimized CALDH. IF: insoluble fraction. SF: soluble fraction. F: fraction.

Maltose-binding protein (MBP) is a widely used fusion tag in recombinant protein expression systems. MBP is commonly fused to target proteins to enhance their solubility, reduce aggregation and inclusion body formation [48]. Additionally, MBP serves as an affinity tag, allowing for the straightforward purification of the fusion protein using amylose resin, which specifically binds MBP. Figure 5 shows the SDS-PAGE analysis of the mbp-CALDH. The mbp-CALDH, with an expected molecular weight of approximately 75 kDa, was predominantly found in the soluble fraction of the cell lysate, with a smaller portion present in the insoluble fraction. The wide band observed at 75 kDa in the eluted fractions 2 and 3 corresponds to the target protein, which appears spread out due to its high concentration. However, additional bands in the 37-50 kDa range were also present, indicating the presence of lower molecular weight impurities. A significant amount of protein near 75kDa was also detected in the flowthrough during the initial purification. The flowthrough was collected and subjected to another round of purification using the same column. The purified flow is low in yield but with less impurity and the flowthrough in this purification still showed a significant amount of protein at around 75 kda band.

The maltose binding protein significantly improves the expression and solubility of CALDH. However, the presence of proteins other than the target protein could be due to several factors. Some endogenous proteins expressed by BL21 may bind nonspecifically to the amylose column. Additionally, mbp-CALDH might be partially degraded by host cell proteases. The degradation

products that still attached to the mbp tag can bind to the column and be eluted during purification, resulting in smaller molecular weight bands on SDS-PAGE. The presence of protein at the 75 kDa band in the flowthrough indicated that a large portion of the mbp-CALDH passed through the amylose column, which potentially exceeded the binding capacity of the amylose column [48, 49]. Another possible reason is that cells grown in LB medium may produce substantial amounts of amylase, which can competitively inhibit MBP from binding to the amylose column. This amylase may release maltose, further preventing the target protein from effectively binding to the column[48, 50]. It has been reported that using MBP for protein expression can lead to some impurities after affinity purification based on the MBP tag. To achieve higher purity, it is often necessary to cleave the MBP tag from the recombinant protein after the initial purification. Following the cleavage, the target protein can be further purified using a secondary affinity tag or other purification methods specific to the target protein, thereby removing the MBP and any associated impurities and achieving a higher level of purity for the final product. [50].

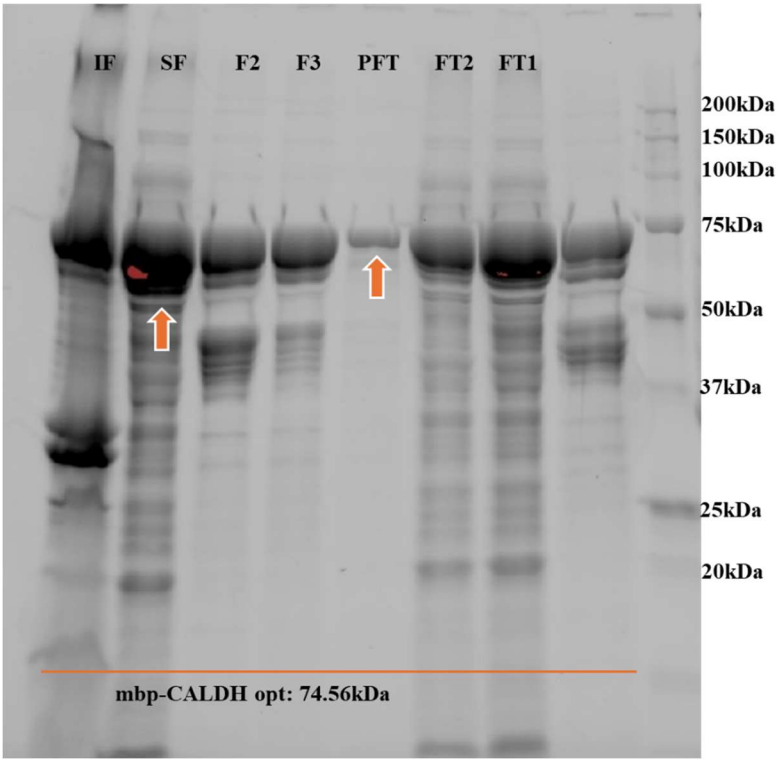

Figure 4. SDS-PAGE result of mbp-CALDH. IF: insoluble fraction. SF: soluble fraction. F: fraction. PFT: purified flowthrough. FT: flowthrough.

3.3 Characterization of mbp-CALDH

3.3.1 Cofactor Specificity

The objective of this experiment was to investigate the efficiency of the conversion of FFCA to FDCA with different cofactors, NAD^+ and $NADP^+$. To explore cofactor specificity of mbp-CALDH, two concentrations of FFCA (1 mM and 5 mM) were tested with either NAD^+ or $NADP^+$ as the cofactor. The HPLC chromatography shows an interference at retention time of FDCA when used $NADP^+$ as cofactor, thus the alteration in FFCA level was used for discussion. The graph shows the FFCA concentrations remaining after 24 hours under the different experimental conditions. For both 1 mM (0.14mg/mL) and 5 mM (0.7mg/mL) FFCA concentrations, the groups using $NADP^+$ as the cofactor exhibited over 5 times higher FFCA consumed compared to those using NAD^+. Specifically, the highest FFCA consumption was observed in the 5 mM FFCA group with $NADP^+$, reaching approximately 0.22 mg/mL. The 5 mM FFCA group with NAD^+ showed a slightly lower consumption, around 0.15 mg/mL. For the 1 mM FFCA conditions, the FFCA concentrations were lower overall, with $NADP^+$ still leading to marginally higher conversion than NAD^+. While both cofactors can be effective, the economic advantages of NAD^+ outweigh the marginal efficiency gains provided by $NADP^+$. Thus, NAD^+ was deemed more suitable for further experiments due to its lower cost.

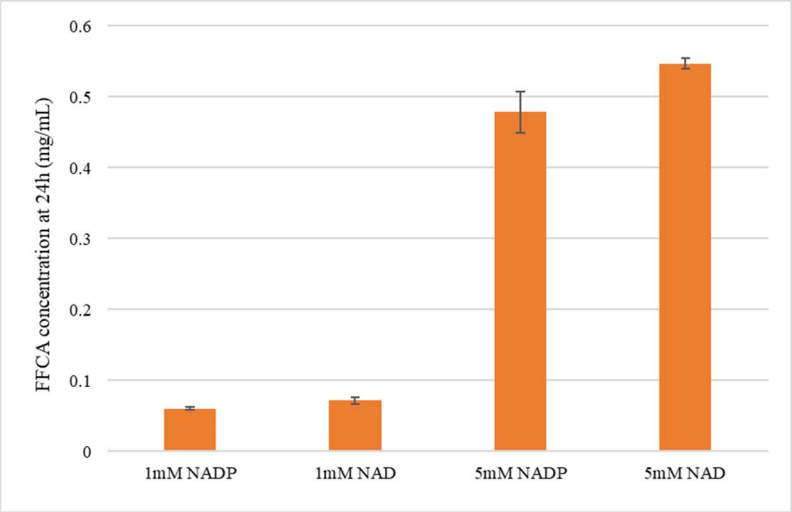

Figure 5. FFCA after 24 hours catalyzed by mbp-CALDH with different cofactors and concentration

3.3.2 Substrate Specificity

To test if mbp-CALDH has ability to oxidize the aldehyde group of other chemicals, different substrates were tested in same concentrations (5mM). With HMF as substrate, the concentration of substrate fluctuated to a certain extent in the first 10 hours (Figure 7). After 24 hours, the

concentration of HMF decreased with low production of HMFCA. The chromatography result from HPLC (Figure 8) shows there are peaks appearing at retention times of 4.0 and 3.0, which might indicate the HMFCA was further oxidized to FFCA and FDCA. With HMFCA as substrate, there was no conversion of HMFCA throughout 24 hours (Figure 9), the fluctuation of concentration may be attributed to the evaporation of the solution during the incubation. These findings suggest that mbp-CALDH can indeed oxidize HMF, converting it initially to HMFCA and potentially further to FFCA and FDCA.

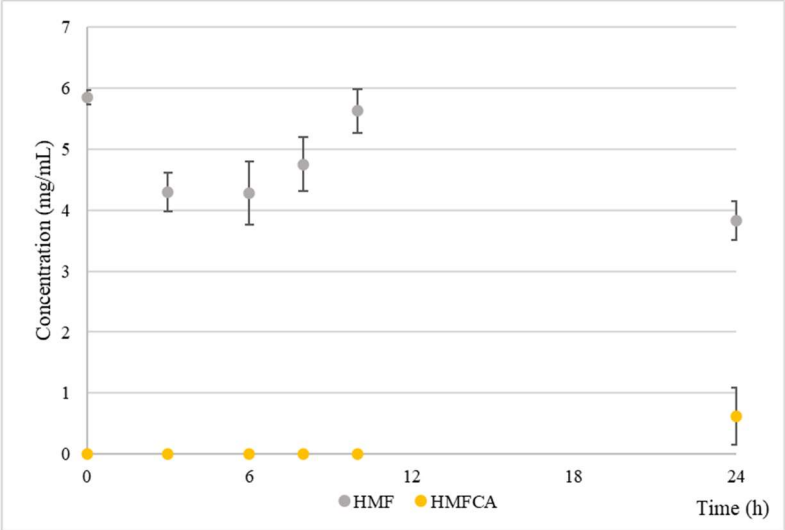

Figure 6. The conversion of HMF catalyzed by mbp-CALDH

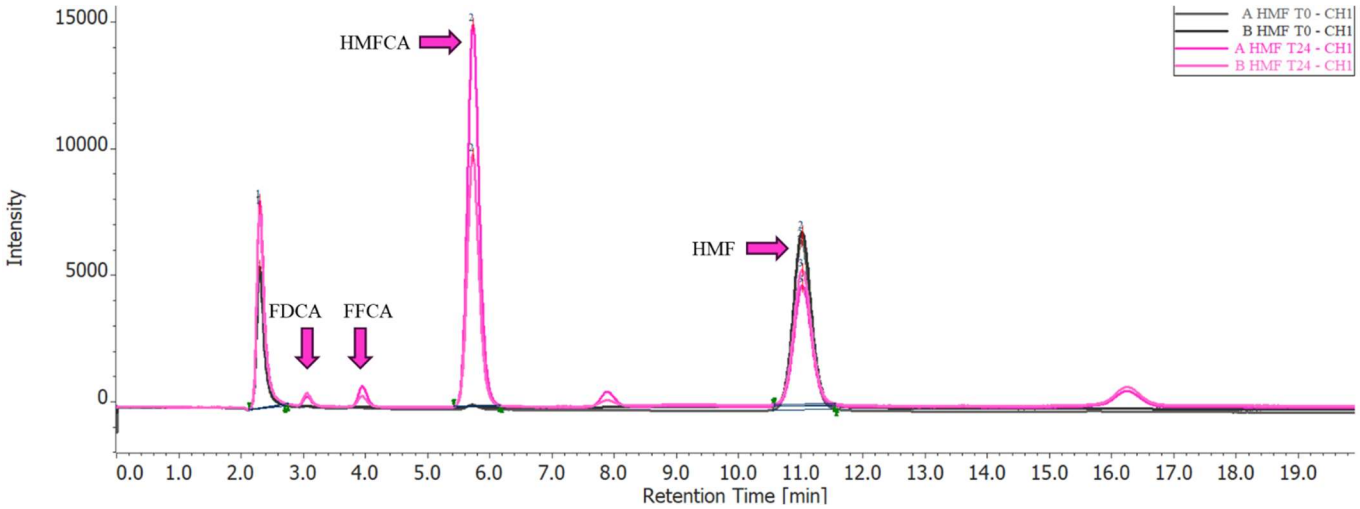

Figure 7. HPLC analysis results of CALDH catalyzed oxidation of HMF in 24 hours

Combining the result from HMF as substrate and HMFCA as substrate, it can be seen HMFCA produced from HMF can be further oxidized to FFCA and FDCA. While with HMFCA as

substrate, there is no conversion. One possible explanation could be the toxicity of HMFCA [51]. As previously reported, at a specific concentration of HMFCA, whole cell biocatalysts have shown reduced or completely loss in activity, which would apply to the pure enzymes. When HMFCA is directly used as substrate, the high concentration of HMFCA inactivated the enzyme while when HMF was used as substrate, the HMFCA was produced gradually which reduces its toxic, and the enzyme can catalyse the subsequent reactions to produce FFCA and FDCA.

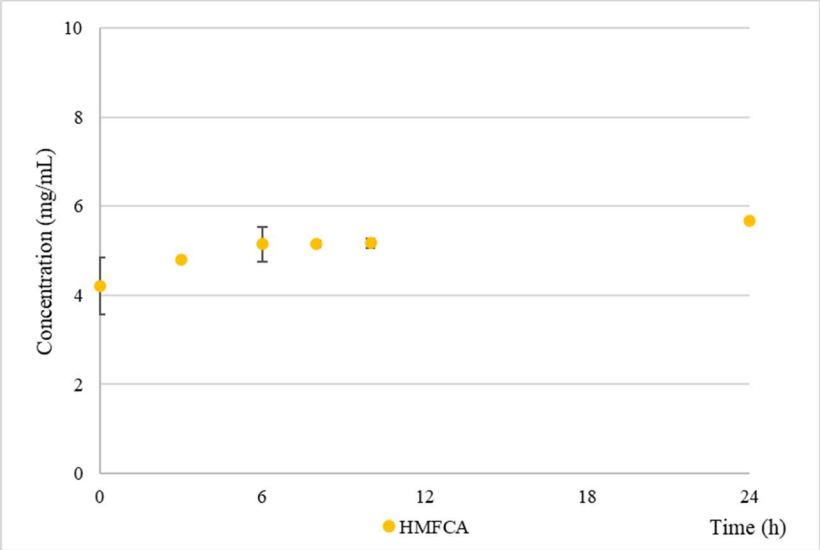

Figure 8. The conversion of HMFCA catalyzed by mbp-CALDH

When furfural was used as the substrate, its concentration decreased over the first ten hours, eventually leading to complete conversion. HPLC analysis revealed a new peak at a retention time of 7.9 minutes, suggesting that the aldehyde group in furfural was oxidized to a hydroxyl group, likely forming 2-furoic acid. Unfortunately, due to the unavailability of furoic acid in the lab, we were unable to confirm this peak.

When comparing the conversion of HMF and furfural, it is clear that furfural starts converting within the first ten hours, whereas most of the HMF conversion happens after ten hours. The explanation can the availability of the substrate. Compared to HMF, furfural has a smaller molecular size and lacks the hydroxymethyl group. The homologous structure model of CALDH indicates that the active site of the enzyme may be hydrophobic, the interaction between active site and substrates like HMF and furfural is influenced significantly by their functional groups. Furfural contains an aldehyde group and is relatively small and less polar, which allows it to better align with and access a hydrophobic active site. As a result, furfural has a faster initial reaction

rates. In contrast, HMF has another more polar and bulkier hydroxymethyl group which might be hindered by the hydrophobic active site, resulting in the lag phase in the first ten hours.

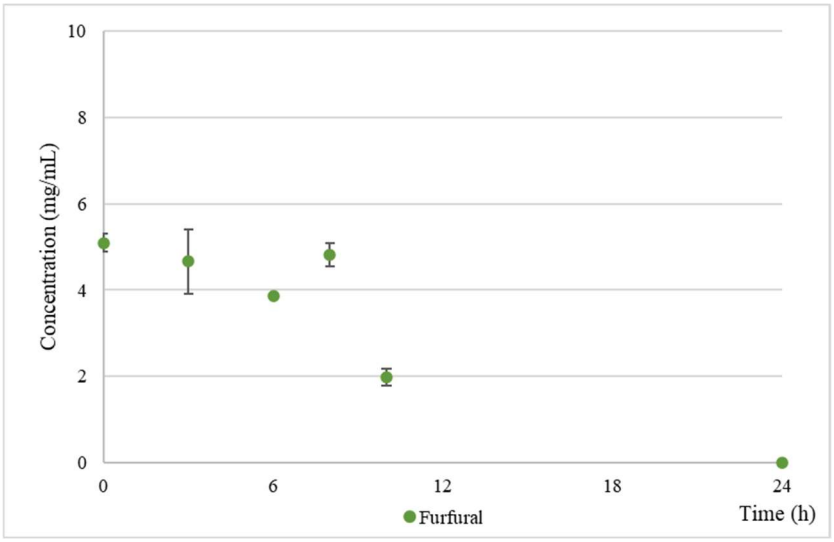

Figure 9. The conversion of furfural catalyzed by mbp-CALDH

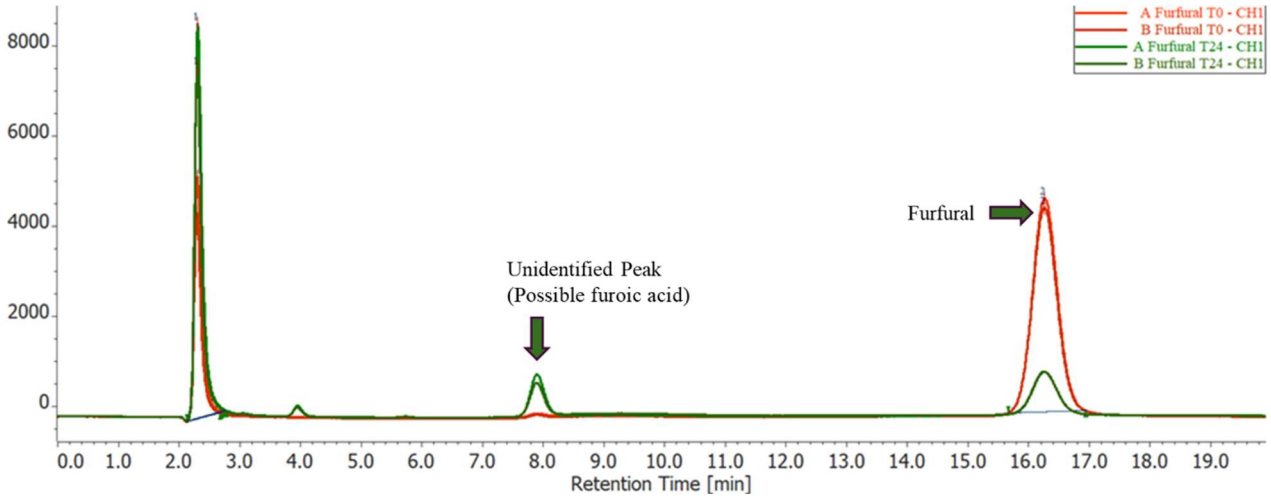

Figure 10. HPLC analysis results of CALDH catalyzed oxidation of furfural in 24 hours

In conclusion, when catalyzed by mbp-CALDH, furfural achieved a complete conversion rate of 100%. In comparison, FFCA and HMF were partially converted, with conversion rates around 35%, while HMFCA showed no conversion. The non-conversion of HMFCA can be caused by the toxicity of HMFCA.

HMFCA has been demonstrated to exert substantial inhibition and toxicity to whole cells, primarily attributed to its acidity [51]. In this study, the pH alteration caused by HMFCA is likely to decrease the enzyme activity of mbp-CALDH and leads to the lack of conversion. The further oxidation of HMFCA at low concentration, as shown in Figure 8, supports the hypothesis. To better understand whether HMFCA can act as a substrate for CALDH, experiments using different concentrations of HMFCA can be conducted. Additionally, toxicity of furan derivatives were reported [52]. A whole-cell system could help protect the enzyme from high concentration of furan derivatives, which is expected to improve both substrate tolerance and conversion efficiency and leads to higher yields, However, the accumulation of HMFCA above certain limit can inhibit the whole cells as well [51]. Given that mbp-CALDH is capable of oxidizing furfural, it raises an interesting question about whether it can also oxidize DFF, a similar compound to furfural with an additional aldehyde group to FFCA and then oxidized to FDCA (Scheme 1). Experiments could be designed where DFF is used as a substrate with similar conditions to those used for furfural.

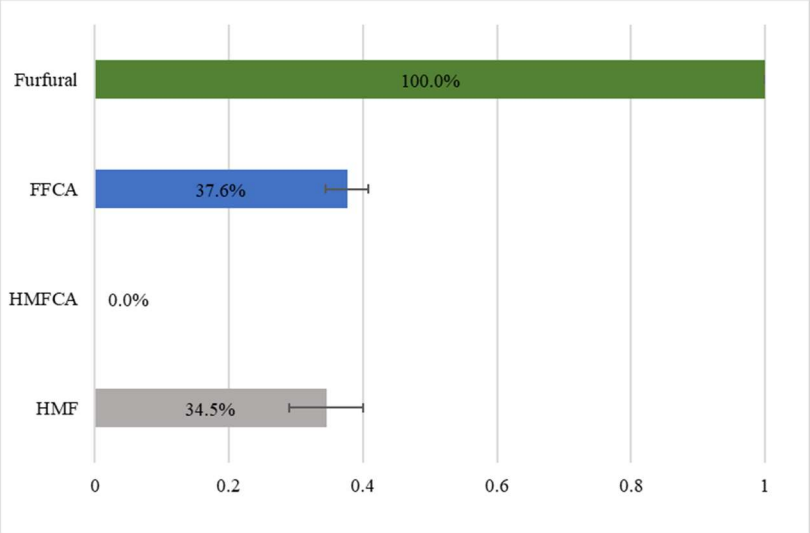

Figure 11. The conversion when 5mM of HMF, HMFCA, FFCA and furfural as substrate and catalyzed by mbp-CALDH

3.3.3 mbp-CALDH activity at different substrate (FFCA) concentration

In this experiment, the effect of different substrate (FFCA) concentrations on the conversion efficiency of FFCA to FDCA was studied at a fixed enzyme concentration of 150 μM. The results showed that as the substrate concentration increased, the conversion rate in 24 hours significantly decreased, at 1mM FFCA the conversion was highest with a conversion of 86.1%. The reaction with 14mM FFCA has a second high conversion of 47%. When the substrate concentration

reached 20mM, the conversion dropped to 19.8% and using 50mM substrate concentration, there was no conversion detected after 24 hours. When examining the FDCA conversion in terms of mass, it becomes evident that the 47% conversion of 14 mM FFCA produced 0.92 mg/mL of FDCA, which is significantly higher than the 0.12 mg/mL yield from the 86.1% conversion of 1 mM FFCA. However, the 20 mM FFCA resulted in a lower yield of 0.56 mg/mL of FDCA compared to the 14 mM substrate. Despite the lower conversion in percentages, higher initial substrate concentrations can yield more FDCA in mass, up to a certain threshold.

At lower substrate concentrations, the enzyme exhibits higher conversion efficiency, indicating that it functions under optimal conditions and processes the available substrate effectively without significant inhibition or saturation. However, as the substrate concentration increases, the conversion efficiency decreases remarkably. This decline occurs as enzyme approaching its saturation point, where the available enzymes are fully occupied and unable to process additional substrate molecules effectively [53]. This decrease could also be due to substrate inhibition, where at high substrate concentrations, two or more substrate molecules simultaneously bind to the active site and forms a substrate-enzyme-product complex, which considerably reduce the enzyme's catalytic activity [54]. At higher concentrations, FFCA may occupy the active site without catalysis occurring, likely due to inhibitory effects from its aldehyde group. This inhibition could also affect the mass transport of the substrate and the product, further slowing down the overall catalytic process. [54]. Additionally, product inhibition may impact the conversion rate. Given the structural similarity between FFCA and FDCA, the product might also have high affinity to the enzyme and potentially acting as a competitive inhibitor [55]. These combined factors result in mbp-CALDH to deviate from the standard Michaelis-Menten kinetics as substrate concentration increases, leading to a more complex relationship between substrate concentration and reaction rate than the Michaelis-Menten presents.

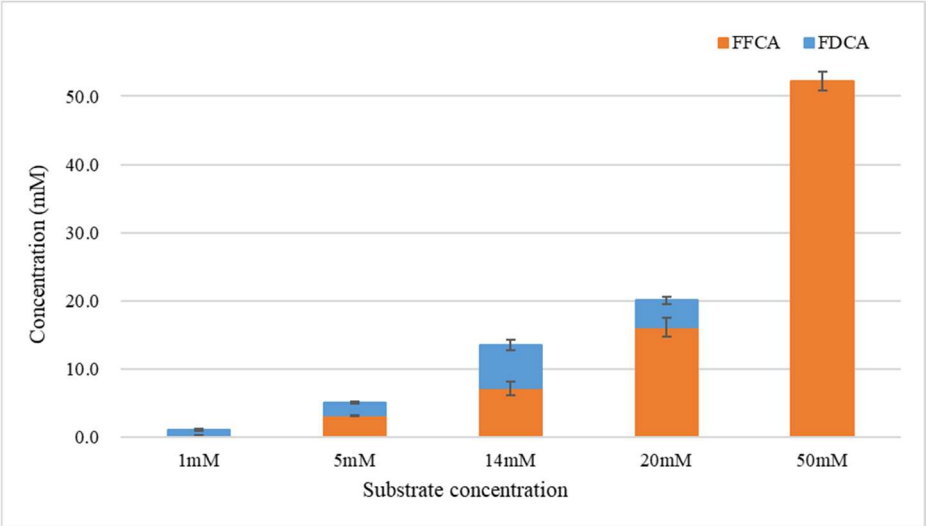

Figure 12. Effect of FFCA concentration on conversion catalyzed by mbp-CALDH

3.3.4 FFCA conversion at different enzyme concentration

This experiment was designed to evaluate the efficiency of FFCA conversion to FDCA using varying concentrations of mbp-CALDH, with a fixed initial concentration of FFCA at 5 mM. Figure 13 illustrates the conversion rates of FFCA to FDCA at different mbp-CALDH enzyme concentrations, ranging from 50 µM to 1.5 mM. At the lowest enzyme concentration of 50 µM, the conversion percentage was around 55% and when the enzyme concentration was increased to 100 µM, the conversion rate improved significantly to approximately 78%. At higher enzyme concentrations of 300 µM, 600 µM, and 1.5 mM, the FFCA was fully converted to FDCA within 24 hours, achieving a 100% conversion in all three cases.

The experiment demonstrates that when catalyzed by mbp-CALDH, the conversion rate of FFCA increases with enzyme concentration. As the enzyme concentration increased from 50 µM to 300 µM, the enzyme was not fully saturated with the available substrate, so increasing the enzyme concentration meant that more enzyme molecules were available to interact with the substrate, thereby increasing the reaction rate. Beyond 300 µM enzyme concentration, the reaction reaches a point where the enzyme is relatively excessive to the substrate and leads to the full conversion without limitation of enzyme availability.

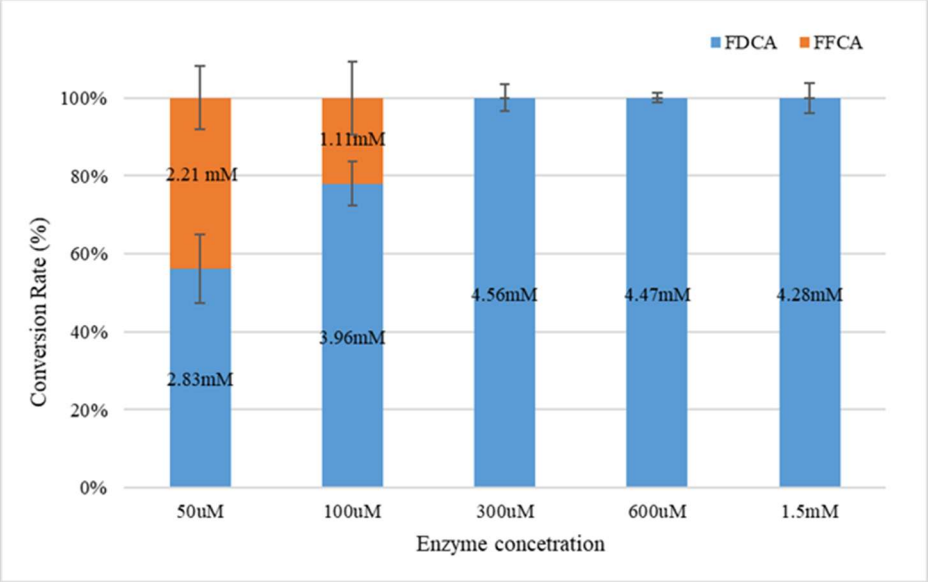

Figure 13. Effect of enzyme concentration on conversion catalyzed by mbp-CALDH

3.4 FFCA conversion with cofactor regeneration

In this experiment, we investigated the impact of nox on the conversion of FFCA to FDCA under conditions of limited NAD^+ availability. Two experimental groups were established: one with nox to facilitate the regeneration of NAD^+, and a control group without nox. The aim was to compare the efficiency of FDCA production over a 24-hour period, thereby assessing the role of nox in enhancing the biocatalytic conversion process. The graph illustrates the FDCA production (in mg/mL) over time for both experimental conditions (Figure 15). The group with nox displayed a significant increase in FDCA production, ultimately achieving more than three times the conversion rate compared to the group without nox at the 24-hour point. The results from this experiment clearly demonstrate the significant impact of cofactor regeneration exhibited by nox on the conversion of FFCA to FDCA, particularly under conditions of limited NAD^+ availability. It is expected that increase in FDCA production rate would be even more significant with NADP+ as the cofactor.

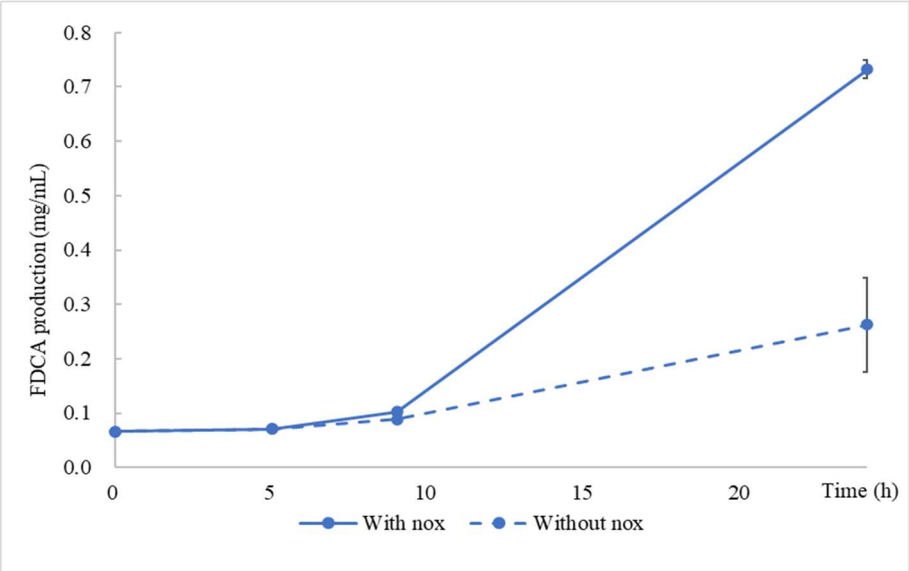

Figure 14. FDCA production catalyzed by mbp-CALDH with and without cofactor regeneration system

3.5 Co-Expression Vector Design for NOX and mbp-CALDH

Since NOX was found to positively impact the activity of CALDH, a duet vector was constructed to co-express both NOX and mbp-CALDH. After constructing the final vector that potentially includes NOX and mbp-CALDH, the vector was sent for Sanger sequencing using the forward primer for NOX, the forward primer for mbp-CALDH, and the universal reverse primer for the

T7 terminator. The sequencing results were analyzed using SnapGene, and the analysis confirmed that both NOX and mbp-CALDH were successfully cloned into the pRSFDuet vector. The confirmation that both genes were correctly inserted into the vector suggests that the cloning process was successful. The pRSFDuet vector carrying Nox and mbp-CALDH will be transformed into BL21(DE3) cells and after confirming successful transformation and expression, BL21(DE3) cells can be used for whole-cell catalysis.

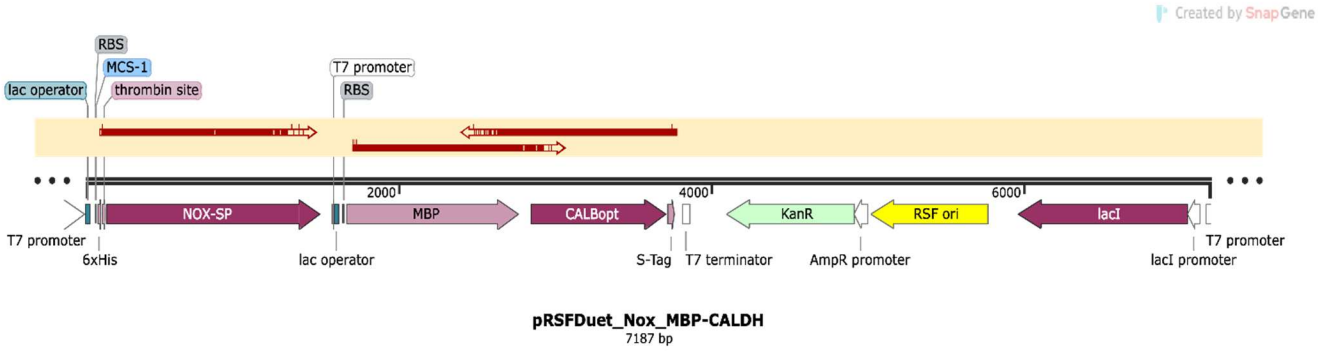

Figure 15. The sequencing result analyzed by SnapGene.

4 Conclusions and Future work

This thesis explores the characterization of Coniferyl Aldehyde Dehydrogenase (CALDH) and the implementation of a NAD^+ regeneration system using NADH oxidase to enhance the biotransformation process from 5-Formyl-2-furancarboxylic Acid (FFCA) to 2,5-furandicarboxylic acid (FDCA). In this study, mbp-CALDH and NADH oxidase were successfully expressed and purified. It was demonstrated that mbp-CALDH can utilize both NAD^+ and $NADP^+$ as cofactors and oxidize substrates such as HMF, FFCA, and furfural. Additionally, detailed experiments were conducted to assess the conversion rate of FFCA to FDCA under different substrate and enzyme concentrations over a 24-hour period, providing valuable insights into the catalytic capabilities of mbp-CALDH. The results showed that the NAD^+ regeneration system significantly improved FDCA yield, increasing it by threefold, addressing the challenge of cofactor limitations in enzymatic reactions. Moreover, a co-expression vector containing both NOX and mbp-CALDH was successfully constructed, achieving a key objective of the thesis.

However, due to time constraints, several aspects of the research could not be explored further. Specifically, the expression and purification of mbp-CALDH did not yield high-purity enzyme

preparations, and the optimal storage conditions for mbp-CALDH were not thoroughly investigated. Additionally, the kinetic parameters of mbp-CALDH when using FFCA as a substrate were not determined, limiting our understanding of the enzyme's full catalytic potential.

Future research should focus on further purification of mbp-CALDH to achieve higher purity levels and enable more accurate determination of its kinetic parameters, especially with FFCA as a substrate. The co-expression system that was successfully constructed should be transformed into a suitable host for whole-cell catalysis experiments, allowing for a comparison of FFCA conversion efficiency between strains containing only mbp-CALDH and those co-expressing NOX and mbp-CALDH. Additionally, it is worth investigating the potential oxidation of HMFCA observed in preliminary experiments, which could be achieved by conducting a series of experiments with varying HMFCA and enzyme concentrations. The oxidation of furfural can be also further studied, but confirming the product would require running a furoic acid standard through HPLC. Expanding the substrate scope to include other aromatic compounds like DFF could also reveal new catalytic capabilities of mbp-CALDH.

5 Acknowledgement

I would like to sincerely thank my supervisor, Dr. Mohamed Ismail, for his unwavering guidance and support throughout this research. His expertise and encouragement have been invaluable to the success of this thesis. I am also grateful to my examiner, Professor Rajni Hatti-Kaul, for her insightful feedback and suggestions, which greatly improved the quality of my work. A special thanks to Dr. Mahmoud Sayed Ali and Dr. Adel Elsayed Attia Abouhmad, who provided me with significant help and guidance during times when my supervisor was unavailable. Your assistance was crucial to the progress of my research. A heartfelt thank you to my colleagues and friends in the Division of Biotechnology for their support and to the technical staff for their assistance in the lab. Finally, I want to express my deepest gratitude to my family for their continuous support and encouragement.

References

[1] ‘Plastics – the fast Facts 2023 • Plastics Europe’, *Plastics Europe*. [Online]. Available: https://plasticseurope.org/knowledge-hub/plastics-the-fast-facts-2023/. [Accessed: 20-Aug-2024]

[2] ‘Plastics - the Facts 2022 • Plastics Europe’, *Plastics Europe*. [Online]. Available: https://plasticseurope.org/knowledge-hub/plastics-the-facts-2022/. [Accessed: 20-Aug-2024]

[3] Maocai Shen, Wei Huang, Ming Chen, Biao Song, Guangming Zeng, and Yaxin Zhang, ‘(Micro)plastic crisis: Un-ignorable contribution to global greenhouse gas emissions and climate change’, *J. Clean. Prod.*, vol. 254, p. 120138, May 2020. DOI: 10.1016/j.jclepro.2020.120138

[4] J. Y. Zhu and Xuejun Pan, ‘Efficient sugar production from plant biomass: Current status, challenges, and future directions’, *Renew. Sustain. Energy Rev.*, vol. 164, p. 112583, Aug. 2022. DOI: 10.1016/j.rser.2022.112583

[5] Catherine Rosenfeld, Johannes Konnerth, Wilfried Sailer-Kronlachner, Pia Solt, Thomas Rosenau, and Hendrikus W. G. van Herwijnen, ‘Current Situation of the Challenging Scale-Up Development of Hydroxymethylfurfural Production’, *ChemSusChem*, vol. 13, no. 14, pp. 3544–3564, 2020. DOI: 10.1002/cssc.202000581

[6] Rajni Hatti-Kaul, Lars J. Nilsson, Baozhong Zhang, Nicola Rehnberg, and Stefan Lundmark, ‘Designing Biobased Recyclable Polymers for Plastics’, *Trends Biotechnol.*, vol. 38, no. 1, pp. 50–67, Jan. 2020. DOI: 10.1016/j.tibtech.2019.04.011

[7] ‘2 5 Furandicarboxylic Acid Fdca Market’. [Online]. Available: https://www.reportsanddata.com/report-detail/2-5-furandicarboxylic-acid-fdca-market. [Accessed: 12-Jul-2024]

[8] Ed de Jong, Hendrikus (Roy) A. Visser, Ana Sousa Dias, Clare Harvey, and Gert-Jan M. Gruter, ‘The Road to Bring FDCA and PEF to the Market’, *Polymers*, vol. 14, no. 5, p. 943, Jan. 2022. DOI: 10.3390/polym14050943

[9] Mahmoud Sayed, Yasser Gaber, Fredrik Junghus, Eric Valdés Martín, Sang-Hyun Pyo, and Rajni Hatti-Kaul, ‘Oxidation of 5-hydroxymethylfurfural with a novel aryl alcohol oxidase from Mycobacterium sp. MS1601’, *Microb. Biotechnol.*, vol. 15, no. 8, pp. 2176–2190, Mar. 2022. DOI: 10.1111/1751-7915.14052

[10] Deyang Zhao, Ting Su, Yantao Wang, Rajender S. Varma, and Christophe Len, 'Recent advances in catalytic oxidation of 5-hydroxymethylfurfural', *Mol. Catal.*, vol. 495, p. 111133, Nov. 2020. DOI: 10.1016/j.mcat.2020.111133

[11] Shivshankar Prasad, Al Jaradah Khalid, Vivek Narishetty, Vinod Kumar, Suman Dutta, and Ejaz Ahmad, 'Recent advances in the production of 2,5-furandicarboxylic acid from biorenewable resources', *Mater. Sci. Energy Technol.*, vol. 6, pp. 502–521, Jan. 2023. DOI: 10.1016/j.mset.2023.04.005

[12] Frank Koopman, Nick Wierckx, Johannes H. de Winde, and Harald J. Ruijssenaars, 'Identification and characterization of the furfural and 5-(hydroxymethyl)furfural degradation pathways of Cupriavidus basilensis HMF14', *Proc. Natl. Acad. Sci.*, vol. 107, no. 11, pp. 4919–4924, Mar. 2010. DOI: 10.1073/pnas.0913039107

[13] Anna Weimer, Michael Kohlstedt, Daniel C. Volke, Pablo I. Nikel, and Christoph Wittmann, 'Industrial biotechnology of Pseudomonas putida: advances and prospects', *Appl. Microbiol. Biotechnol.*, vol. 104, no. 18, pp. 7745–7766, 2020. DOI: 10.1007/s00253-020-10811-9

[14] Frank Koopman, Nick Wierckx, Johannes H. de Winde, and Harald J. Ruijssenaars, 'Efficient whole-cell biotransformation of 5-(hydroxymethyl)furfural into FDCA, 2,5-furandicarboxylic acid', *Bioresour. Technol.*, vol. 101, no. 16, pp. 6291–6296, Aug. 2010. DOI: 10.1016/j.biortech.2010.03.050

[15] Haibo Yuan, Yanfeng Liu, Xueqin Lv, Jianghua Li, Guocheng Du, Zhongping Shi, and Long Liu, 'Enhanced 2,5-furandicarboxylic acid (FDCA) production in RaoultellaornithinolyticaBF60 by manipulation of the key genes in FDCA biosynthesis pathway', vol. 28, no. 12, pp. 1999–2008, Dec. 2018. DOI: 10.4014/jmb.1808.08057

[16] Haibo Yuan, Jianghua Li, Hyun-dong Shin, Guocheng Du, Jian Chen, Zhongping Shi, and Long Liu, 'Improved production of 2,5-furandicarboxylic acid by overexpression of 5-hydroxymethylfurfural oxidase and 5-hydroxymethylfurfural/furfural oxidoreductase in *Raoultella ornithinolytica* BF60', *Bioresour. Technol.*, vol. 247, pp. 1184–1188, Jan. 2018. DOI: 10.1016/j.biortech.2017.08.166

[17] Monika Krystof, María Pérez-Sánchez, and Pablo Domínguez de María, 'Lipase-Mediated Selective Oxidation of Furfural and 5-Hydroxymethylfurfural', *ChemSusChem*, vol. 6, no. 5, pp. 826–830, 2013. DOI: 10.1002/cssc.201200954

[18] Shane M. McKenna, Silke Leimkühler, Susanne Herter, Nicholas J. Turner, and Andrew J. Carnell, 'Enzyme cascade reactions: synthesis of furandicarboxylic acid (FDCA) and carboxylic acids using oxidases in tandem', *Green Chem.*, vol. 17, no. 6, pp. 3271–3275, Jun. 2015. DOI: 10.1039/C5GC00707K

[19] Alexander Karich, Sebastian B. Kleeberg, René Ullrich, and Martin Hofrichter, 'Enzymatic Preparation of 2,5-Furandicarboxylic Acid (FDCA)—A Substitute of Terephthalic Acid—By the Joined Action of Three Fungal Enzymes', *Microorganisms*, vol. 6, no. 1, p. 5, Jan. 2018. DOI: 10.3390/microorganisms6010005

[20] Mahmoud Sayed, Sang-Hyun Pyo, Nicola Rehnberg, and Rajni Hatti-Kaul, 'Selective Oxidation of 5-Hydroxymethylfurfural to 5-Hydroxymethyl-2-furancarboxylic Acid Using Gluconobacter oxydans', *ACS Sustain. Chem. Eng.*, vol. 7, no. 4, pp. 4406–4413, Feb. 2019. DOI: 10.1021/acssuschemeng.8b06327

[21] Kwabena Owusu Danquah and Daniel Gyamfi, 'Chapter 3 - Alcohol and Aldehyde Dehydrogenases: Molecular Aspects', in *Molecular Aspects of Alcohol and Nutrition*, V. B. Patel, Ed. San Diego: Academic Press, 2016, pp. 25–43 [Online]. DOI: 10.1016/B978-0-12-800773-0.00003-3

[22] Raquel Pequerul, Javier Vera, Joan Giménez-Dejoz, Isidro Crespo, Joan Coines, Sergio Porté, Carme Rovira, Xavier Parés, and Jaume Farrés, 'Structural and kinetic features of aldehyde dehydrogenase 1A (ALDH1A) subfamily members, cancer stem cell markers active in retinoic acid biosynthesis', *Arch. Biochem. Biophys.*, vol. 681, p. 108256, Mar. 2020. DOI: 10.1016/j.abb.2020.108256

[23] Natalie Lassen, J. Bronwyn Bateman, Tia Estey, Jer R. Kuszak, David W. Nees, Joram Piatigorsky, Gregg Duester, Brian J. Day, Jie Huang, Lisa M. Hines, and Vasilis Vasiliou, 'Multiple and Additive Functions of ALDH3A1 and ALDH1A1: CATARACT PHENOTYPE AND OCULAR OXIDATIVE DAMAGE IN Aldh3a1(-/-)/Aldh1a1(-/-) KNOCK-OUT MICE*', *J. Biol. Chem.*, vol. 282, no. 35, pp. 25668–25676, Aug. 2007. DOI: 10.1074/jbc.M702076200

[24] Kim Shortall, Ahmed Djeghader, Edmond Magner, and Tewfik Soulimane, 'Insights into Aldehyde Dehydrogenase Enzymes: A Structural Perspective', *Front. Mol. Biosci.*, vol. 8, May 2021 [Online]. DOI: 10.3389/fmolb.2021.659550

[25] Sandra Achterholt, Horst Priefert, and Alexander Steinbüchel, 'Purification and Characterization of the Coniferyl Aldehyde Dehydrogenase from Pseudomonas sp. Strain HR199 and Molecular Characterization of the Gene', *J. Bacteriol.*, vol. 180, no. 17, pp. 4387–4391, Sep. 1998.

[26] Jörg Overhage, Alexander Steinbüchel, and Horst Priefert, 'Biotransformation of Eugenol to Ferulic Acid by a Recombinant Strain of Ralstonia eutropha H16', *Appl. Environ. Microbiol.*, vol. 68, no. 9, pp. 4315–4321, Sep. 2002. DOI: 10.1128/AEM.68.9.4315-4321.2002

[27] ‘b-Nicotinamide adenine dinucleotide 20111-18-6’. [Online]. Available: http://www.sigmaaldrich.com/. [Accessed: 17-Jul-2024]

[28] Masako Higuchi, Yuji Yamamoto, and Yoshiyuki Kamio, ‘Molecular biology of oxygen tolerance in lactic acid bacteria: Functions of NADH oxidases and Dpr in oxidative stress’, *J. Biosci. Bioeng.*, vol. 90, no. 5, pp. 484–493, Jan. 2000. DOI: 10.1016/S1389-1723(01)80028-1

[29] Carmela M. Gibson, T. Conn Mallett, Al Claiborne, and Michael G. Caparon, ‘Contribution of NADH Oxidase to Aerobic Metabolism of *Streptococcus pyogenes*’, *J. Bacteriol.*, vol. 182, no. 2, pp. 448–455, Jan. 2000. DOI: 10.1128/JB.182.2.448-455.2000

[30] Hui Gao, Jinglin Li, Dakshinamurthy Sivakumar, Tae-Su Kim, Sanjay K. S. Patel, Vipin C. Kalia, In-Won Kim, Ye-Wang Zhang, and Jung-Kul Lee, ‘NADH oxidase from *Lactobacillus reuteri*: A versatile enzyme for oxidized cofactor regeneration’, *Int. J. Biol. Macromol.*, vol. 123, pp. 629–636, Feb. 2019. DOI: 10.1016/j.ijbiomac.2018.11.096

[31] George T. Lountos, Rongrong Jiang, William B. Wellborn, Tracey L. Thaler, Andreas S. Bommarius, and Allen M. Orville, ‘The Crystal Structure of NAD(P)H Oxidase from Lactobacillus sanfranciscensis: Insights into the Conversion of O2 into Two Water Molecules by the Flavoenzyme’, *Biochemistry*, vol. 45, no. 32, pp. 9648–9659, Aug. 2006. DOI: 10.1021/bi060692p

[32] Martina Sudar, Zvjezdana Findrik, Marija Vuković Domanovac, and Đurđa Vasić-Rački, ‘Coenzyme regeneration catalyzed by NADH oxidase from *Lactococcus lactis*’, *Biochem. Eng. J.*, vol. 88, pp. 12–18, Jul. 2014. DOI: 10.1016/j.bej.2014.04.001

[33] Mesfin Angaw Tesfay, Xin Win, Huibin Lin, Yujie Liu, Can Li, Jianqiang Lin, and Jianqun Lin, ‘Efficient L-xylulose production using whole-cell biocatalyst with NAD+ regeneration system through co-expression of xylitol dehydrogenase and NADH oxidase in *Escherichia coli*’, *Biochem. Eng. J.*, vol. 175, p. 108137, Nov. 2021. DOI: 10.1016/j.bej.2021.108137

[34] Hui Gao, Manish Kumar Tiwari, Yun Chan Kang, and Jung-Kul Lee, ‘Characterization of H2O-forming NADH oxidase from *Streptococcus pyogenes* and its application in l-rare sugar production’, *Bioorg. Med. Chem. Lett.*, vol. 22, no. 5, pp. 1931–1935, Mar. 2012. DOI: 10.1016/j.bmcl.2012.01.049

[35] Ho-Jin Park, Christian O. A. Reiser, Simone Kondruweit, Helmut Erdmann, Rolf D. Schmid, and Mathias Sprinzl, ‘Purification and characterization of a NADH oxidase from the thermophile Thermus thermophilus HB8’, *Eur. J. Biochem.*, vol. 205, no. 3, pp. 881–885, 1992. DOI: 10.1111/j.1432-1033.1992.tb16853.x

[36] Xianqin Yang and Kesen Ma, 'Purification and characterization of an NADH oxidase from extremely thermophilic anaerobic bacterium Thermotoga hypogea', *Arch. Microbiol.*, vol. 183, no. 5, pp. 331–337, Aug. 2005. DOI: 10.1007/s00203-005-0777-6

[37] Masako Higuchi, Mamoru Shimada, Yoshikazu Yamamoto, Tetsuya Hayashi, Toshihiko Koga, and Yoshiyuki Kamio, 'Identification of two distinct NADH oxidases corresponding to H2O2-forming oxidase and H2O-forming oxidase induced in Streptococcus mutans', *Microbiology*, vol. 139, no. 10, pp. 2343–2351, 1993. DOI: 10.1099/00221287-139-10-2343

[38] Katherine Y. King, Joshua A. Horenstein, and Michael G. Caparon, 'Aerotolerance and Peroxide Resistance in Peroxidase and PerR Mutants of Streptococcus pyogenes', *J. Bacteriol.*, vol. 182, no. 19, pp. 5290–5299, Oct. 2000.

[39] Fei-Long Li, Ying Shi, Jiu-Xun Zhang, Jian Gao, and Ye-Wang Zhang, 'Cloning, expression, characterization and homology modeling of a novel water-forming NADH oxidase from *Streptococcus mutans* ATCC 25175', *Int. J. Biol. Macromol.*, vol. 113, pp. 1073–1079, Jul. 2018. DOI: 10.1016/j.ijbiomac.2018.03.016

[40] Werner Hummel and Bettina Riebel, 'Isolation and biochemical characterization of a new NADH oxidase from'.

[41] Bettina R. Riebel, Phillip R. Gibbs, William B. Wellborn, and Andreas S. Bommarius, 'Cofactor Regeneration of NAD+ from NADH: Novel Water-Forming NADH Oxidases', *Adv. Synth. Catal.*, vol. 344, no. 10, pp. 1156–1168, 2002. DOI: 10.1002/1615-4169(200212)344:10<1156::AID-ADSC1156>3.0.CO;2-#

[42] Hui Gao, Manish Kumar Tiwari, Raushan Kumar Singh, Bong Hyun Sung, Sun Chang Kim, and Jung-Kul Lee, 'Role of surface residue 184 in the catalytic activity of NADH oxidase from Streptococcus pyogenes', *Appl. Microbiol. Biotechnol.*, vol. 98, no. 16, pp. 7081–7088, Aug. 2014. DOI: 10.1007/s00253-014-5666-y

[43] Mingguang Yan, Weibing Yin, Xiao Fang, Jianjun Guo, and Hong Shi, 'Characteristics of a water-forming NADH oxidase from Methanobrevibacter smithii, an archaeon in the human gut', *Biosci. Rep.*, vol. 36, no. 6, p. e00410, Nov. 2016. DOI: 10.1042/BSR20160357

[44] Hugo G. Menzella, 'Comparison of two codon optimization strategies to enhance recombinant protein production in Escherichia coli', *Microb. Cell Factories*, vol. 10, no. 1, p. 15, Mar. 2011. DOI: 10.1186/1475-2859-10-15

[45] Michael P. Malakhov, Michael R. Mattern, Oxana A. Malakhova, Mark Drinker, Stephen D. Weeks, and Tauseef R. Butt, 'SUMO fusions and SUMO-specific protease for efficient expression and purification of proteins', *J. Struct. Funct. Genomics*, vol. 5, no. 1, pp. 75–86, Mar. 2004. DOI: 10.1023/B:JSFG.0000029237.70316.52

[46] Tauseef R. Butt, Suzanne C. Edavettal, John P. Hall, and Michael R. Mattern, 'SUMO fusion technology for difficult-to-express proteins', *Protein Expr. Purif.*, vol. 43, no. 1, pp. 1–9, Sep. 2005. DOI: 10.1016/j.pep.2005.03.016

[47] Rafael S. Chagas, Felipe A. M. Otsuka, Mario A. R. Pineda, Roberto K. Salinas, and Sandro R. Marana, 'Mechanism of imidazole inhibition of a GH1 β-glucosidase', *FEBS Open Bio*, vol. 13, no. 5, pp. 912–925, Mar. 2023. DOI: 10.1002/2211-5463.13595

[48] Mario Lebendiker and Tsafi Danieli, 'Purification of Proteins Fused to Maltose-Binding Protein', in *Protein Chromatography: Methods and Protocols*, D. Walls and S. T. Loughran, Eds. Totowa, NJ: Humana Press, 2011, pp. 281–293 [Online]. DOI: 10.1007/978-1-60761-913-0_15

[49] 'MBPTrap HP', *Cytiva*. [Online]. Available: https://www.cytivalifesciences.com/en/us/shop/chromatography/prepacked-columns/affinity-tagged-protein/mbptrap-hp-p-00306?srsltid=AfmBOopYdrYzn0sOQh9FQhsbu9eoiPdbBctbyv_RhfiadMFrVrSaD68u. [Accessed: 21-Aug-2024]

[50] 'Troubleshooting Guide for NEBExpress® MBP Fusion and Purification System (NEB #E8201) | NEB'. [Online]. Available: https://www.neb.com/en/tools-and-resources/troubleshooting-guides/troubleshooting-guide-for-nebexpress-mbp-fusion-and-purification-system-neb-e8201. [Accessed: 21-Aug-2024]

[51] Shizeng Wang, Gang Cheng, Chijioke Joshua, Zijun He, Xinxiao Sun, Ruimin Li, Lexuan Liu, and Qipeng Yuan, 'Furfural tolerance and detoxification mechanism in Candida tropicalis', *Biotechnol. Biofuels*, vol. 9, no. 1, p. 250, Nov. 2016. DOI: 10.1186/s13068-016-0668-x

[52] Tobias Modig, Gunnar Lidén, and Mohammad J Taherzadeh, 'Inhibition effects of furfural on alcohol dehydrogenase, aldehyde dehydrogenase and pyruvate dehydrogenase.', *Biochem. J.*, vol. 363, no. Pt 3, pp. 769–776, May 2002.

[53] Masataka Yoshino and Keiko Murakami, 'Analysis of the substrate inhibition of complete and partial types', *SpringerPlus*, vol. 4, p. 292, Jun. 2015. DOI: 10.1186/s40064-015-1082-8

[54] Piia Kokkonen, Andy Beier, Stanislav Mazurenko, Jiri Damborsky, David Bednar, and Zbynek Prokop, 'Substrate inhibition by the blockage of product release and its control by tunnel engineering', *RSC Chem. Biol.*, vol. 2, no. 2, pp. 645–655. DOI: 10.1039/d0cb00171f

[55] Yan Liu, Fan Zhang, Ling Jiang, J. Jefferson P. Perry, Zhihe Zhao, and Jiayu Liao, 'Product inhibition kinetics determinations - Substrate interaction affinity and enzymatic kinetics

using one quantitative FRET assay', *Int. J. Biol. Macromol.*, vol. 193, pp. 1481–1487, Dec. 2021. DOI: 10.1016/j.ijbiomac.2021.10.211

Appendix A:

Table A1. Components of PCR reaction with Phusion DNA polymerase

Component	Volume
5X Phusion HF Buffer	10µL
10mM dNTPs	1µL
Forward primer	2.5µL
Reverse primer	2.5µL
Template DNA	2.5µL
Phusion High-Fidelity DNA polymerase	0.5µL
Water, nuclease-free	add to 50µL
Total volume	50µL

Table A2. Cycle condition of PCR reaction with Phusion DNA polymerase

Cycle step	Temperature (°C)	Time	Cycle
Initial denaturation	98	30s	1
Denaturation	98	10s	
Annealing	70	30s	35
Extension	72	1min	
Final extension	72	10min	1

Table A3. Components of colony PCR

Component	Volume
DreamTaq PCR Master Mix (2X)	10µL
Forward primer	0.5µL
Reverse primer	0.5µL
Template DNA (Single colony)	10pg-1µg
Water, nuclease-free	10µL
Total volume	10µL

Table A4. Cycle condition of colony PCR

Cycle step	Temperature (°C)	Time	Cycle
Initial denaturation	95	5min	1
Denaturation	95	30s	
Annealing	70	30s	35
Extension	72	1min	
Final extension	72	10min	1

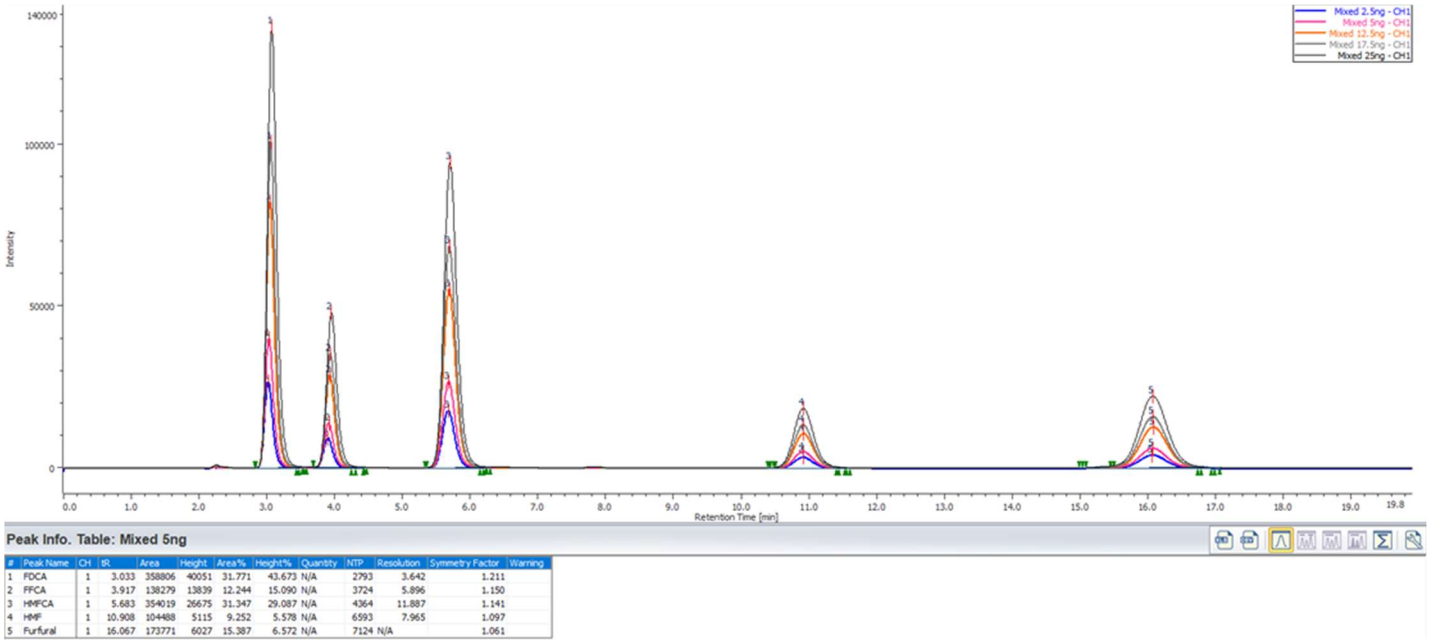

#	Peak Name	CH	tR	Area	Height	Area%	Height%	Quantity	NTP	Resolution	Symmetry Factor	Warning
1	FDCA	1	3.033	358806	40051	31.771	43.673	N/A	2793	3.642	1.211	
2	FFCA	1	3.917	138279	13839	12.244	15.090	N/A	3724	5.896	1.150	
3	HMFCA	1	5.683	354019	26675	31.347	29.087	N/A	4364	11.887	1.141	
4	HMF	1	10.908	104488	5115	9.252	5.578	N/A	6593	7.965	1.097	
5	Furfural	1	16.067	173771	6027	15.387	6.572	N/A	7124	N/A	1.061	

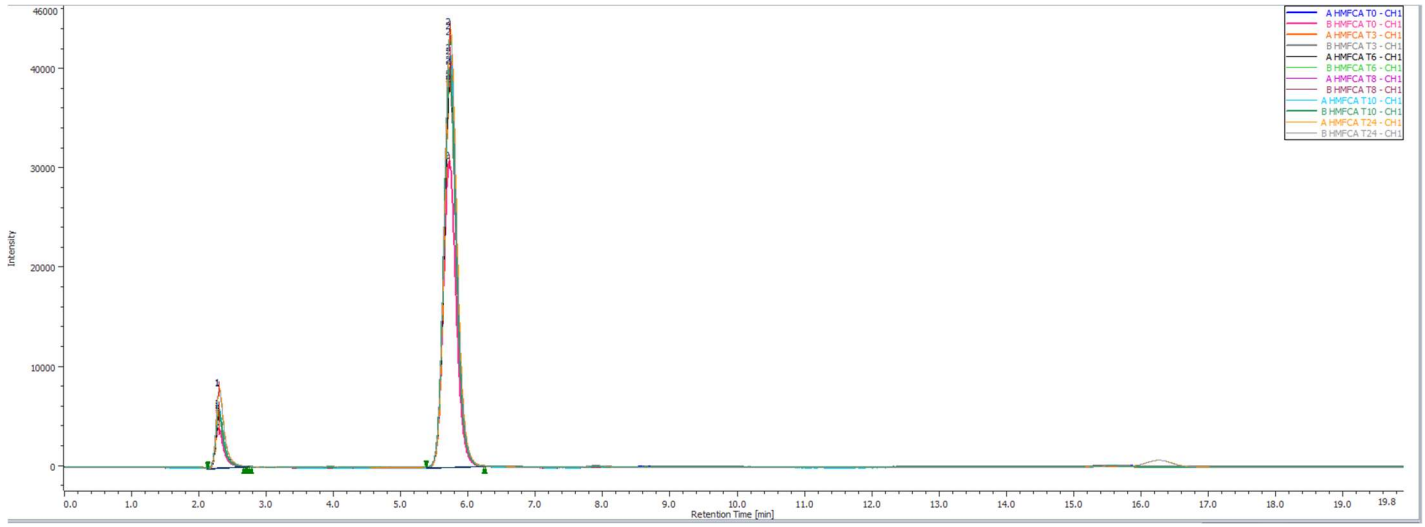

Figure A 1. HPLC analysis results of CALDH catalyzed oxidation of HMFCA in 24 hours